The Cocos and Carnegie Aseismic Ridges: a Trace Element Record of Long-term Plume–Spreading Center Interaction

KAREN S. HARPP[1]*, VIRGINIA D. WANLESS[1]†, ROBERT H. OTTO[1]‡, KAJ HOERNLE[2] AND REINHARD WERNER[3]

[1]DEPARTMENT OF GEOLOGY, COLGATE UNIVERSITY, 13 OAK DRIVE, HAMILTON, NY 13346, USA

[2]DYNAMICS OF THE OCEAN CRUST, IfM-GEOMAR, WISCHHOFSTR. 1–3, 24148 KIEL, GERMANY

[3]TETHYS GEOCONSULTING GmbH, WISCHHOFSTR. 1–3, 24148 KIEL, GERMANY

RECEIVED JULY 10, 2003; ACCEPTED JULY 29, 2004
ADVANCE ACCESS PUBLICATION OCTOBER 24, 2004

The aseismic Cocos and Carnegie Ridges, two prominent bathymetric features in the eastern Pacific, record ~20 Myr of interaction between the Galápagos hotspot and the adjacent Galápagos Spreading Center. Trace element data determined by inductively coupled plasma-mass spectrometry in >90 dredged seamount lavas are used to estimate melt generation conditions and mantle source compositions along the ridges. Lavas from seamount provinces on the Cocos Ridge are alkalic and more enriched in incompatible trace elements than any in the Galápagos archipelago today. The seamount lavas are effectively modeled as small degree melts of a Galápagos plume source. Their eruption immediately follows the failure of a rift zone at each seamount province's location. Thus the anomalously young alkalic lavas of the Cocos Ridge, including Cocos Island, are probably caused by post-abandonment volcanism following either a ridge jump or rift failure, and not the direct activity of the Galápagos plume. The seamounts have plume-like signatures because they tap underlying mantle previously infused with Galápagos plume material. Whereas plume heterogeneities appear to be long-lived, tectonic rearrangements of the ridge plate boundary may be the dominant factor in controlling regional eruptive behavior and compositional variations.

KEY WORDS: *mantle plume; mid-ocean ridge; Galápagos; abandoned rift; partial melting of the mantle*

INTRODUCTION

Most aseismic ridges are considered to represent the long-term history of hotspot activity as a tectonic plate passes over a mantle plume (e.g. Morgan, 1971). The Cocos and Carnegie Ridges, located in the eastern Pacific Ocean, have likewise been attributed to the Galápagos plume (Fig. 1; Holden & Dietz, 1972). In this case, however, the system has been complicated by the proximity of the hotspot to the Galápagos Spreading Center (GSC). Because the ridge has been migrating northeastward for more than the past 5 Myr (Wilson & Hey, 1995) and migrated southward before that (Meschede & Barckhausen, 2000), volcanic material from the plume has been erupted variably onto both the Nazca and Cocos plates. Consequently, the accumulated lavas of the Cocos and Carnegie Ridges constitute a record of interaction between the Galápagos plume and the Galápagos Spreading Center for close to 20 Myr (e.g. Werner *et al.*, 1999).

The present-day Galápagos archipelago exhibits an anomalously wide variety of geochemical compositions, from enriched, hotspot-like signatures in the west and south to mid-ocean ridge basalt (MORB)-like lavas in the central and northern regions. The spatial zonation has been attributed to a heterogeneous plume and to extensive interaction between the plume and the asthenosphere (e.g. White & Hofmann, 1978; Geist *et al.*, 1988; White *et al.*, 1993; Harpp & White, 2001). One of the controversial questions about the Galápagos system is whether the geochemical zonation in the present-day archipelago is a long-term phenomenon related to inherent plume heterogeneity (Hoernle *et al.*, 2000) or only the recent result of upper-mantle contamination.

Because of the complex tectonic relationship between the Galápagos Spreading Center and the Galápagos

*Corresponding author. Telephone: (315)228-7211. Fax: (315)228-7187. E-mail: kharpp@mail.colgate.edu
†Present address: Department of Geology and Geophysics, SOEST, University of Hawaii, Honolulu, HI 96822, USA.
‡Present address: University of Miami, Rosenstiel School of Marine and Atmospheric Science, Miami, FL 33149, USA.

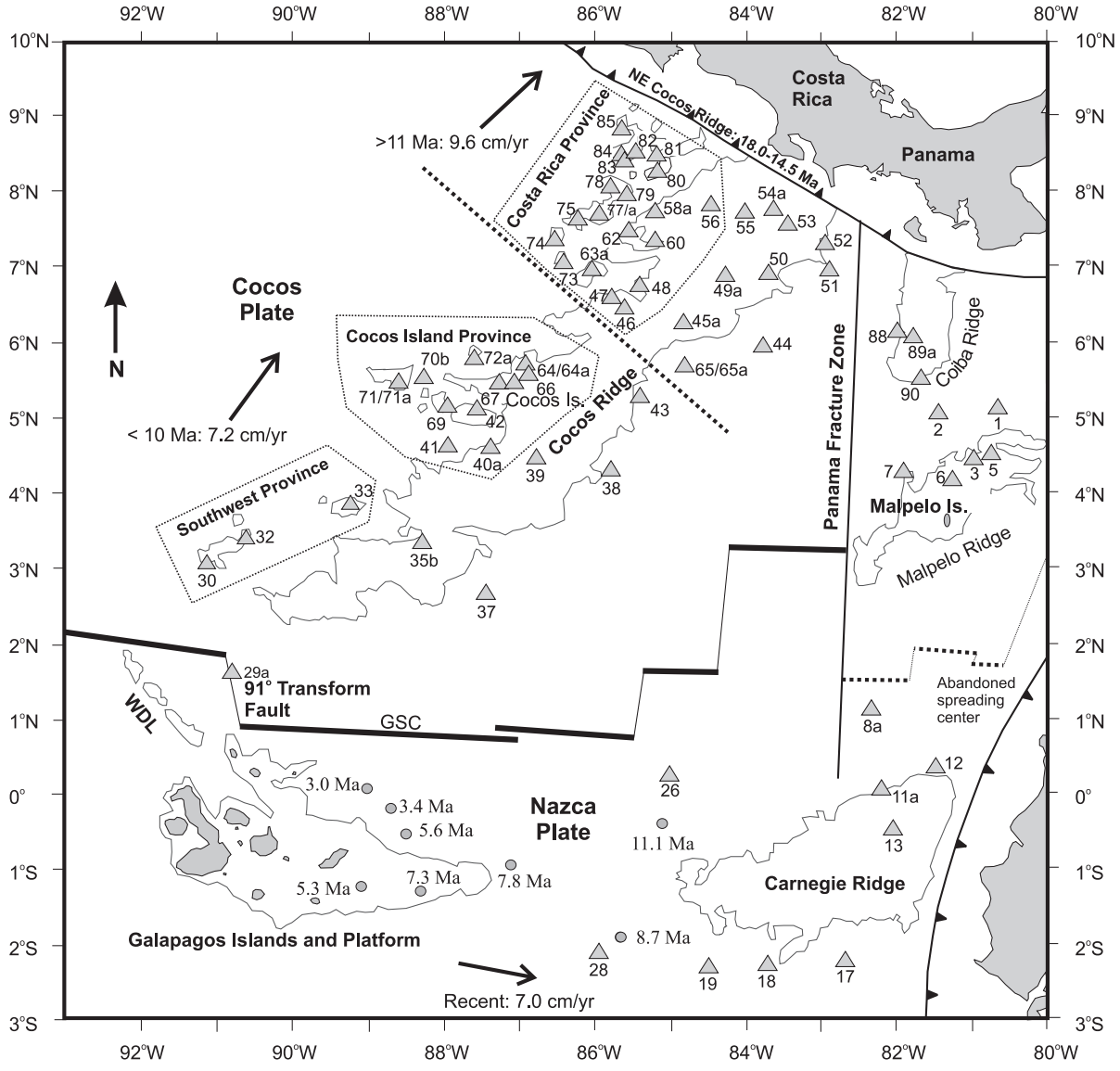

Fig. 1. Map of the study area, including dredge locations on the Cocos, Carnegie, Coiba, and Malpelo Ridges from *Sonne* cruise SO 144-3 of the PAGANINI expedition. Contour line is for 2000 m below sea level (Smith & Sandwell, 1997). Grey circles are a selection of dated dredges from the PLUME02 cruise (Christie *et al.*, 1992; Sinton *et al.*, 1996). Sources of age data: Cocos Ridge near Costa Rican coast from Werner *et al.* (1999); Malpelo Island from Hoernle *et al.* (2002). Plate motion vectors from Kellogg & Vega (1995). Dashed line marking the ~11–12 Ma lithosphere age on the Cocos Ridge is based on plate motion rates and magnetic data (Wilson, 1996; Barckhausen *et al.*, 2001). GSC, Galápagos Spreading Center; WDL, Wolf–Darwin Lineament. Adapted from Werner *et al.* (2003).

hotspot system, volcanic activity along the Cocos and Carnegie Ridges provides a means of addressing important questions about plume heterogeneity and longevity, as well as plume–ridge interaction dynamics. Seamounts on the Cocos and Carnegie aseismic ridges, as well as the related Malpelo and Coiba ridges were systematically sampled for the first time during dredging operations of the 1999 PAGANINI expedition, R.V. *Sonne* cruise SO 144-3 (Fig. 1). Two of the fundamental goals of the cruise were to document the temporal variations in Galápagos plume composition and eruptive activity over the past >20 Myr, and to determine the extent of plume interaction with the migrating GSC. Here, we present results from over 90 new inductively coupled plasma-mass spectrometry (ICP-MS) trace element analyses of lavas from seamounts along the aseismic ridges and their implications for the dynamic history of the Galápagos plume. Major element and radiogenic isotopic analyses (Sr, Nd, Pb) of the recovered lavas have been reported, along with a discussion of the magnetic profiles collected during the cruise, by Werner *et al.* (2003); hafnium isotopic analyses of selected lavas have been presented by Geldmacher *et al.*

(2003). Additional trace element and isotopic data (Sr, Nd, Pb) from the Cocos Ridge and Costa Rica Seamount Province have been reported by Hoernle *et al.* (2000).

BACKGROUND INFORMATION

Tectonic history

The Galápagos Islands are located on the Equator, ~1000 km west of the South American coast. They emerge from an extensive, shallow submarine volcanic platform that marks the western terminus of the Carnegie Ridge (Fig. 1). The Galápagos Spreading Center lies directly north of the archipelago and marks the boundary between the Nazca and Cocos plates.

The tectonic history of the plume-spreading center system has been summarized by Wilson & Hey (1995), Meschede & Barckhausen (2000), Barckhausen *et al.* (2001) and Werner *et al.* (2003). On the basis of seafloor magnetic anomaly analysis, Barckhausen *et al.* (2001) proposed that spreading initiated on the GSC at 22·7 Ma, causing the breakup of the Farallon plate. At 19·5 Ma, the GSC began a major southward jump, shifting strike by 22° clockwise, where it remained for another 5 Myr. The ridge underwent a second jump south at 14·5 Ma, taking on its current orientation (Meschede & Barckhausen, 2000). Between 14·5 and 9·5 Ma, the Malpelo Ridge was rifted away from the Carnegie Ridge toward its present location. The 14·5 Ma jump was the first in a series of smaller, more frequent southward jumps that continue today (Wilson & Hey, 1995; Barckhausen *et al.*, 2001). The GSC overlay the Galápagos plume between 5 and 9 Ma, but the interactions have been complicated by the multiple southward ridge segment jumps and the formation of the 91°W transform fault at ~3 Ma (Wilson & Hey, 1995). Currently, the GSC is 150–250 km north of the hotspot center, presumed to be located slightly west of Fernandina Island (e.g. Kurz & Geist, 1999). Consequently, the relationship between the plume and the spreading center has varied from a ridge-centered plume to an off-axis configuration over the past ~20 Myr (Wilson & Hey, 1995).

Description of study area

Werner *et al.* (2003) have described the morphology of the study area in detail; only the general features are reviewed here.

The Cocos Plate

The Cocos Ridge, long believed to represent the track of the Cocos Plate over the Galápagos hotspot (e.g. Hey, 1977; Lonsdale & Klitgord, 1978), extends over 1000 km between the 91°W transform fault on the GSC and the west coast of Costa Rica, parallel to the current direction of plate motion (35·5°; Gripp & Gordon, 1990; Fig. 1). The Cocos Ridge reaches elevations of less than 1000 m below sea level, making it the most prominent positive bathymetric feature in the eastern Pacific (e.g. Hey, 1977; Walther, 2003). The NE end of the Cocos Ridge and the adjacent seamounts have been dated at 13·0–14·5 Ma (Werner *et al.*, 1999). The ridge narrows slightly to the SW, decreasing progressively in volume toward its intersection with the GSC. Magnetic anomaly studies indicate that the lithosphere underlying the NE end of the Cocos Ridge ranges in age from 15 Ma in the south to 19 Ma in the north (Barckhausen *et al.*, 2001).

Whereas there is a relatively even distribution of seamounts along the Cocos Ridge crest, the greatest concentration of seamounts is on the NW flank (Fig. 1). More than 30 volcanic structures that reach over 1000 m bathymetrically dominate this region, alongside many additional, smaller seamounts. Werner *et al.* (2003) divided the seamount population along the Cocos Ridge into three regions (Fig. 1): (1) the Costa Rica Seamount Province, the largest with 18 major volcanic structures arranged in three >300 km long chains of seamounts that run parallel to the Cocos Ridge crest; (2) the Cocos Island Province, a cluster of seven major seamounts, Cocos Island, and additional minor structures that extend ~200 km to the west and SW of Cocos Island; (3) the Southwest Seamount Province, six major seamounts scattered along the northern flank of the SW Cocos Ridge.

The Nazca Plate

The Galápagos hotspot track on the Nazca Plate is manifested as the ~600 km long Carnegie Ridge, which is up to 300 km wide at its eastern end (Fig. 1). The Carnegie Ridge is oriented nearly parallel to the direction of Nazca Plate motion (91°; Gripp & Gordon, 1990). Meschede & Barckhausen (2001) estimated that the most ancient parts of the Carnegie Ridge were formed at around 20 Ma. In general, seamounts along the Carnegie Ridge are less abundant than on the Cocos Ridge and rarely reach more than several hundred meters above base level (Werner *et al.*, 2003); they are more abundant and evenly distributed across the eastern part of the ridge and on the Galápagos Platform (Christie *et al.*, 1992), but decrease in number in the bathymetric saddle centered at 86°W. Dredging operations were less successful along the Carnegie Ridge, often yielding no rocks or heavily manganese-encrusted samples.

The Malpelo Ridge is *c.* 300 km long and 100 km wide, trending in a northeasterly direction (Fig. 1; Werner *et al.*, 2003). This structure is believed to be an older section of the Carnegie Ridge (e.g. Hey, 1977; Lonsdale & Klitgord, 1978; Werner *et al.*, 2003), whereas Meschede *et al.* (1998) proposed that it originated as part of the Cocos Ridge. Hoernle *et al.* (2002) reported $^{40}Ar/^{39}Ar$ ages from Malpelo Island ranging from 15·8 to 17·3 Ma.

On the NE Nazca Plate, the Coiba Ridge is a gently sloping, sediment-covered plateau 150 km long by 100 km wide (Fig. 1; Werner *et al.*, 2003). Hoernle *et al.*

(2002) proposed that it is a continuation of the Cocos Ridge that was offset along a paleo-transform fault. Coiba Ridge sediments include fossils that date back to 15 Ma (van Andel *et al.*, 1973).

ANALYTICAL METHODS

During R.V. *Sonne* cruise SO 144-3 (9 November–18 December 1999), we sampled >80 seamounts on the Cocos, Carnegie, Malpelo, and Coiba Ridges (Fig. 1). Most rocks were collected by dredge (DR samples), although a few were acquired with a remotely controlled grab sampler with real-time video (TVG samples). Samples were crushed, sieved (125 μm), and sonicated in de-ionized water to remove fine particles and surface contamination. The chips were examined under a binocular microscope to collect *c.* 10 g of the freshest, most pristine lava fragments. In many instances, the rocks were severely altered. Chips were powdered in agate and split for isotopic, major element, and trace element analysis. For dredges with more than one distinct lithology, several representative samples were processed.

Approximately 250 mg of rock powder were digested in a closed PFA Teflon container with 20 ml HNO_3 and 5 ml HF sample for 40 h (e.g. Harpp, 1995). The solution was then evaporated to dryness. The solid residue was redissolved in 5 ml 50% HNO_3 and diluted 1000-fold in 1% HNO_3. All chemical procedures were conducted in HEPA-filtered Plexiglas clean boxes and all reagents were purified.

Concentrations of the trace elements were determined by ICP-MS using a Hewlett–Packard HP4500 system at Colgate University (Table 1). Measurements were made using an online internal standard correction consisting of a 1:20 dilution of a 1 ppm ^{115}In, ^{133}Cs, and ^{182}W solution. Raw data were corrected to the closest internal standard mass (e.g. Doherty, 1989; Eggins *et al.*, 1997). Contributions from polybaric oxide and doubly charged interferences were consistently below 1%. At least three replicate analyses of each solution were performed; precision and accuracy are represented by multiple analyses of the USGS standard W-2 run as an unknown (Table 2).

Samples selected for geochemistry were first crushed to small pieces, then washed in deionized water and carefully handpicked under a binocular microscope. Rock powders were dried in a furnace at 110°C for 12 h to drive off moisture. Water and CO_2 were analyzed in an IR photometer (Rosemount CSA 5003). Major elements of whole-rock samples were determined on fused beads using a Phillips X'Unique PW1480 X-ray fluorescence spectrometer (XRF) equipped with a Rh-tube at IFM-GEOMAR. Accuracy of international reference standards JB-2, JB-3 and JA-2, measured with the samples, is better than 3% (SiO_2, TiO_2, Al_2O_3, MgO, CaO, K_2O, 4% (Fe_2O_3), P_2O_5), and 10% (Na_2O).

RESULTS

Lavas collected from the Cocos, Carnegie, Malpelo, and Coiba Ridges reveal a wide spectrum of lithologies, ranging from predominant basaltic pillow and sheet flow fragments to volcaniclastic and sedimentary rocks, as well as plutonic samples from the SE Cocos Ridge near the Panama fracture zone (Fig. 1). Major element, isotopic, and petrographic data have been reported by Werner *et al.* (2003). The complete major and trace element dataset is included as Electronic Appendix 1, which may be downloaded from the *Journal of Petrology* website at http://www.petrology.oupjournals.org/.

Severely altered samples

Many of the dredged samples are severely altered. The following criteria were applied to determine which samples should be removed from the dataset prior to interpretation.

(1) Ten lavas with P_2O_5 >1·5 wt % and/or MnO >0·3 wt % and with extensive visible alteration (i.e. zeolite-filled vesicles, major iron staining or olivine alteration, several millimeter-thick manganese oxide crusts or chlorite coatings) have been eliminated from consideration, predominantly from the Costa Rica Seamount Province (DR-5-1, 5-11, 39-2, 48-1, 58a-1, 64a-1, 73-1, 75-1, 77-1, 82-1).

(2) Sample DR-17-1 has extreme levels of Ba and Sr, and its Ba/Th and Sr/Zr are much higher than any lava from the islands or aseismic ridges (White *et al.*, 1993; Harpp & White, 2001). We believe its composition is strongly altered by seawater; this sample is not considered in subsequent discussion either.

Trace element results by region

The spatial and geochemical complexity of our dataset requires that we consider the new trace element results in groups, on the basis of their location, common morphological characteristics, and apparent petrogenetic relationships (Figs 2–5; Table 3).

The Carnegie Ridge (dredges 8a, 11a-13, 17–19, 26, 28, and 29a)

Lavas dredged from the Carnegie Ridge are predominantly tholeiitic basalts, have trace element concentrations characteristic of both MORB and tholeiitic ocean island basalt (OIB) (Fig. 2; Table 3), and a two-fold variation in MgO content (5·11–10·01 wt %; Werner *et al.*, 2003). In general, the lavas follow coherent differentiation trends (e.g. MgO vs TiO_2), but their relatively wide range in radiogenic isotope ratios (ε_{Nd} 5·97–9·77; Werner *et al.*, 2003) precludes a relationship among the sampled lavas by fractional crystallization or partial melting of a single, homogeneous source.

In general, the more depleted lavas are located on the flanks of the ridge, whereas the enriched lavas are on the

Table 1: Trace element concentrations in representative aseismic ridge lavas (in ppm)

Sample:	1-DR-1	3-TVG-4	5-DR-1	8a-DR-1	12-DR-1	17-TVG-1	26-TVG-1	28-DR-1	29a-DR-5	32-DR-1	33-DR-1	35b-DR-1	37-DR-1
Location:	N. of Malpelo Ridge	Malpelo Ridge	Malpelo Ridge	Carnegie Ridge	Carnegie Ridge	Carnegie Ridge	Carnegie Ridge	Carnegie Ridge	Cocos Ridge at 91°W TF	SW Seamount Province	SW Seamount Province	Cocos Ridge main axis	SW Cocos Ridge
Latitude (°N):	5·16	4·47	4·57	1·03	0·4	−2·16	0·3	−2·07	1·59	3·46	3·9	3·38	2·59
Longitude (°W):	80·64	80·91	80·7	82·19	81·45	82·61	84·98	85·92	90·79	90·62	89·23	88·31	87·48
Sc	37·5	53·9	34·5	44·5	52·7	23·7	49·9	56·0	37·3	36·6	41·3	30·3	42·7
V	230	394	434	299	338	350	308	327	280	289	309	211	318
Cr	379	159	17·0	394	446	182	213	69·7	329	96·8	62·2	697	376
Co	41·6	57·4	46·3	48·5	52·5	35·2	41·2	52·9	45·3	35·1	55·8	61·2	47·2
Ni	107	92·1	35·4	143	74·8	80·5	62·8	45·9	150	28·1	109	357	149
Cu	83·7	116	238	75·3	96·0	139	84·5	85·6	94·4	24·9	130	85·3	93·9
Zn	60·5	110	138	76·8	94·2	68·3	83·6	98·1	75·6	103	92·4	85·6	67·5
Rb	5·16	7·98	12·6	2·18	4·45	60·7	1·59	2·12	2·23	3·63	5·37	1·25	0·39
Sr	75·9	158	339	86·1	184	438	187	94·4	118	316	257	129	45·8
Y	21·0	28·8	45·8	30·0	26·9	14·2	32·6	26·9	28·9	37·3	31·1	19·9	26·7
Zr	36·5	96·4	335	60·2	85·9	23·7	104	55·9	82·8	125	138	51·7	49·0
Nb	1·56	11·6	59·7	0·75	8·79	12·5	6·52	2·18	4·55	16·8	18·1	3·12	1·67
Ba	11·8	44·2	236	9·46	40·0	821	21·0	17·6	25·0	67·6	113	56·4	5·98
La	1·57	8·78	38·8	1·47	7·03	2·79	5·69	2·17	3·78	14·4	12·9	2·62	1·59
Ce	4·54	20·1	86·4	5·23	16·7	4·22	15·4	6·25	10·7	26·7	29·1	7·15	5·06
Pr	0·81	2·88	11·4	1·06	2·48	0·64	2·49	1·11	1·79	4·69	4·00	1·18	0·94
Nd	4·49	12·9	46·3	6·17	11·5	2·99	12·3	6·06	9·30	21·8	17·8	6·18	5·50
Sm	1·78	3·66	10·3	2·54	3·42	1·04	3·99	2·37	3·15	5·87	4·75	2·15	2·21
Eu	0·71	1·24	2·96	0·94	1·22	0·47	1·43	0·90	1·15	2·04	1·61	0·85	0·78
Gd	2·61	4·26	9·76	3·67	4·08	1·56	4·93	3·33	4·03	6·65	5·34	2·90	3·26
Tb	0·50	0·74	1·48	0·70	0·72	0·29	0·88	0·64	0·73	1·05	0·90	0·53	0·63
Dy	3·39	4·69	8·46	4·78	4·53	2·06	5·53	4·32	4·68	6·05	5·47	3·37	4·27
Ho	0·76	1·01	1·68	1·07	0·98	0·48	1·19	0·98	1·02	1·21	1·16	0·72	0·98
Er	2·19	2·96	4·42	3·12	2·73	1·49	3·30	2·85	2·86	3·16	3·17	1·99	2·88
Tm	0·33	0·44	0·62	0·47	0·40	0·23	0·48	0·43	0·42	0·43	0·45	0·29	0·44
Yb	2·08	2·75	3·72	3·00	2·46	1·50	2·94	2·75	2·64	2·46	2·82	1·76	2·79
Lu	0·31	0·41	0·54	0·45	0·37	0·23	0·43	0·41	0·39	0·36	0·41	0·26	0·43
Hf	1·11	2·49	7·61	1·68	2·20	0·70	2·65	1·54	2·19	3·36	3·25	1·39	1·47
Ta	0·10	0·68	3·69	0·06	0·52	0·49	0·40	0·14	0·28	1·07	1·07	0·20	0·12
Pb	0·52	0·70	2·27	0·21	0·48	4·80	0·60	0·37	0·33	1·03	0·84	0·23	0·17
Th	0·11	0·92	3·71	0·05	0·65	0·12	0·41	0·14	0·29	1·34	1·29	0·17	0·12
U	0·05	0·16	1·42	0·10	0·23	0·03	1·20	0·17	0·09	0·36	0·42	0·05	0·03
SiO_2 (wt %)*	49·49	47·85	48·13	50·1	49·67	50·61	49·9	51·94	48·93	47·83	51·02	48·43	48·23
MgO (wt %)*	7·33	7·13	4·68	5·37	6·27	5·11	6·44	7·47	8·52	4·62	6·70	11·61	9·18

Table 1: continued

Sample:	38-DR-12	39 DR-2	41-DR-1	42-DR-1	43-DR-1	44-DR-14	46-TVG-1	48-DR-1	51-DR-1	52-DR-1	56-TVG-1	60-DR-2	65a-DR-1
Location:	Cocos Island Province	Cocos Ridge main axis	Cocos Island Province	Cocos Island Province	Cocos Ridge main axis	Cocos Ridge main axis	Costa Rica Seamount Province	Costa Rica Seamount Province	Cocos Ridge main axis	Cocos Ridge main axis	Costa Rica Seamount Province	Costa Rica Seamount Province	Cocos Island Province
Latitude (°N):	4·36	4·51	4·67	5·14	5·31	5·97	6·49	6·8	7	7·38	7·87	7·39	5·74
Longitude (°W):	85·78	86·77	87·91	87·54	85·38	83·67	85·57	85·38	82·86	82·9	84·44	85·19	86·8
Sc	22·0	30·2	34·9	10·0	54·5	52·2	21·5	23·4	46·7	45·4	38·7	26·9	23·5
V	194	227	322	152	440	325	153	308	432	312	279	278	173
Cr	127	654	56·3	1·68	170	375	150	30·6	94·8	217	293	3·98	181
Co	31·9	29·1	38·7	19·8	54·8	52·6	35·3	27·4	49·1	46·2	42·5	34·0	32·9
Ni	102	46·5	44·8	9·35	69·6	84·5	140	42·0	52·4	80·1	95·6	13·1	131
Cu	25·8	25·9	54·5	19·4	114	191	30·5	26·1	176	135	71·8	105	21·7
Zn	75·6	165	89·9	123	156	82·9	68·1	106	117	84·5	102	148	69·9
Rb	38·8	8·41	19·0	47·7	2·35	26·5	34·8	7·22	7·21	0·50	4·43	58·2	20·3
Sr	521	324	516	662	210	68·5	1591	714	117	145	312	383	771
Y	25·4	35·7	30·2	39·7	41·9	25·1	33·5	29·4	46·5	25·9	34·0	61·5	31·7
Zr	199	130	179	438	137	48·4	310	158	195	87·3	174	477	253
Nb	68·5	8·22	35·8	84·9	8·51	2·93	88·3	28·1	20·2	9·08	23·1	87·4	75·8
Ba	498	42·8	251	506	119	8·62	643	181	130	31·8	149	500	587
La	37·6	8·39	22·9	54·9	7·59	2·02	48·8	18·6	15·2	6·52	16·3	57·1	41·7
Ce	68·6	20·2	49·1	109	19·7	5·74	91·4	40·1	35·8	16·3	35·2	121	77·9
Pr	7·84	3·07	6·51	13·3	3·19	1·01	10·8	5·39	5·07	2·35	4·80	15·8	9·43
Nd	29·1	14·9	26·6	52·4	15·8	5·39	41·0	23·0	23·0	11·1	20·6	64·9	36·3
Sm	5·67	5·06	6·15	10·9	5·01	2·06	8·41	5·64	6·42	3·25	5·39	14·4	7·66
Eu	1·83	1·79	1·99	3·34	1·74	0·77	2·67	1·90	1·99	1·14	1·78	3·89	2·48
Gd	5·26	6·30	6·10	9·61	6·17	2·89	7·66	5·70	7·56	3·88	5·90	13·7	7·07
Tb	0·79	1·09	0·94	1·40	1·09	0·55	1·11	0·88	1·32	0·70	0·97	2·02	1·02
Dy	4·46	6·51	5·39	7·46	6·87	3·72	6·11	4·94	8·22	4·34	5·90	11·2	5·67
Ho	0·90	1·32	1·08	1·42	1·47	0·84	1·19	0·98	1·78	0·93	1·22	2·17	1·10
Er	2·38	3·40	2·87	3·55	4·16	2·61	3·08	2·45	5·04	2·59	3·35	5·69	2·83
Tm	0·35	0·48	0·40	0·50	0·61	0·40	0·43	0·33	0·75	0·38	0·48	0·77	0·39
Yb	2·11	2·84	2·36	3·01	3·75	2·49	2·56	1·98	4·65	2·41	2·92	4·57	2·34
Lu	0·32	0·40	0·34	0·44	0·56	0·38	0·37	0·28	0·70	0·36	0·43	0·65	0·34
Hf	4·20	3·69	4·15	9·43	3·56	1·40	6·52	3·70	4·70	2·18	4·08	10·5	5·44
Ta	3·81	0·57	2·17	4·87	0·54	0·17	4·91	1·72	1·19	0·55	1·40	5·40	4·16
Pb	2·01	0·78	1·64	2·73	0·55	0·29	2·27	2·39	0·57	0·42	1·00	2·97	1·94
Th	5·27	1·11	2·22	6·71	0·52	0·09	6·85	1·74	1·58	0·67	1·58	5·99	5·20
U	1·28	1·96	0·44	1·42	1·51	0·05	1·60	3·27	0·55	0·30	0·27	1·98	1·35
SiO_2 (wt %)*	47·8	46·11	48·88	50·84	48·62	49·53	47·01	41·57	48·41	49·28	50·81	51·6	46·68
MgO (wt %)*	6·13	2·90	4·87	3·14	5·95	8·04	6·72	2·42	5·93	7·65	6·05	3·15	7·04

Sample:	67-DR-1	69-DR-1	70b-DR-1	74-DR-1	77a-DR-1	78-DR-1	80-DR-1	90-DR-8	Cocos 24	Cocos 33
Location:	Cocos Island Province	Cocos Island Province	Cocos Island Province	Costa Rica Seamount Province	Costa Rica Seamount Province	Costa Rica Seamount Province	Costa Rica Seamount Province	Coiba Ridge	Cocos Island	Cocos Island
Latitude (°N):	5·5	5·21	5·57	7·38	7·76	8·11	8·28	5·54	5·54	5·54
Longitude (°W):	87·26	87·95	88·23	86·52	85·93	85·79	85·15	87·09	87·09	87·09
Sc.0	23·7	30·0	13·3	35·4	36·0	32·5	35·1	39·0	8·45	27·7
V	207	246	81·5	302	332	268	250	324	17·3	247
Cr	227	389	31·7	29·5	12·6	151	682	114	0·68	220
Co	43·9	44·3	7·14	32·6	42·8	43·3	42·7	44·2	2·68	32·7
Ni	159	162	11·4	37·3	16·5	94·3	160	69·0	0·53	84·5
Cu	30·4	46·0	11·0	46·8	37·6	91·1	76·6	155	6·59	19·8
Zn	86·2	76·1	119	108	109	87·3	90·6	93·5	91·2	66·0
Rb	34·4	28·3	110	14·3	18·2	13·2	17·0	1·87	91·1	15·8
Sr	620	401	192	344	326	433	575	272	187	671
Y	30·0	26·3	71·3	35·0	39·5	30·5	24·1	30·0	31·1	30·4
Zr	266	184	836	179	211	205	200	140	947	274
Nb	62·7	45·6	172	26·2	27·9	36·7	51·1	18·0	118	70·1
Ba	435	345	396	215	200	213	271	58·1	1428	416
La	35·0	24·8	106·0	18·1	18·1	22·1	32·3	13·5	67·0	40·0
Ce	69·4	53·1	210	39·0	41·2	47·1	69·4	31·0	124	79·5
Pr	8·68	6·77	25·7	5·13	5·71	6·47	8·90	4·36	13·9	10·0
Nd	34·8	27·5	95·0	22·2	25·6	26·9	36·1	18·9	47·9	40·0
Sm	7·60	6·02	18·3	5·73	6·73	6·34	7·28	4·97	8·54	8·46
Eu	2·43	1·86	2·12	1·93	2·26	2·04	2·23	1·66	3·08	2·62
Gd	7·06	5·61	15·1	6·25	7·31	6·28	6·46	5·38	6·79	7·70
Tb	1·03	0·85	2·27	1·01	1·19	0·97	0·90	0·90	1·01	1·09
Dy	5·58	4·75	12·7	5·92	6·99	5·53	4·73	5·35	5·57	5·87
Ho	1·05	0·97	2·50	1·22	1·44	1·09	0·89	1·10	1·11	1·11
Er	2·68	2·57	6·73	3·27	3·90	2·87	2·27	2·97	3·07	2·75
Tm	0·37	0·37	0·98	0·46	0·55	0·40	0·30	0·42	0·46	0·37
Yb	2·15	2·29	6·09	2·78	3·29	2·36	1·77	2·55	2·93	2·18
Lu	0·31	0·33	0·91	0·41	0·47	0·34	0·25	0·37	0·45	0·31
Hf	5·67	3·96	17·7	4·18	5·04	4·65	4·47	3·47	16·0	5·99
Ta	3·48	2·64	9·03	1·54	1·69	2·27	3·14	1·13	6·61	4·16
Pb	1·86	1·34	5·61	1·42	1·26	1·37	1·67	0·88	4·06	1·55
Th	4·15	2·70	12·9	1·72	1·66	2·25	3·45	1·27	10·4	4·67
U	1·11	0·77	3·32	1·77	0·48	0·60	1·60	0·39	2·48	1·23
SiO_2 (wt %)*	47·46	46·5	60·24	50·64	51·01	49·06	49·13	48·41	60·57	45·78
MgO (wt %)*	7·89	8·83	1·21	4·97	4·86	5·98	8·04	5·96	0·48	7·07

DR, dredge; TVG, video grab sampler; TF, transform fault.
*XRF data from Werner *et al.* (2003) and K. Hoernle & R. Werner (personal communication, 2004).

Table 2: Trace element concentrations in USGS Standard Reference Material W-2 (run as an unknown; in ppm)

	Sc	V	Cr	Co	Ni	Cu	Zn	Rb	Sr	Y	Zr	Nb	Ba
W-2	36·6	270	92·7	44·8	71·4	104	73·9	20·1	193	22·5	87·9	7·8	168
RSD (%)	4·0	3·2	4·5	4·6	5·0	3·9	3·0	4·1	4·1	2·7	3·3	3·4	2·9
Count	22	22	22	28	28	28	28	28	28	26	28	28	28

	La	Ce	Pr	Nd	Sm	Eu	Gd	Tb	Dy	Ho	Er	Tm	Yb	Lu
W-2	10·6	22·7	3·03	12·8	3·31	1·07	3·65	0·61	3·79	0·80	2·25	0·33	2·02	0·30
RSD (%)	3·1	2·9	2·9	2·7	2·9	2·8	2·8	2·8	2·7	2·6	2·6	2·6	2·6	2·4
Count	28	28	28	28	28	28	28	28	28	28	28	28	28	28

	Hf	Ta	Pb	Th	U
W-2	2·27	0·48	8·17	2·13	0·48
RSD (%)	2·6	2·8	6·0	4·3	7·2
Count	28	28	28	28	28

main crest (Figs 3–5). Thus, the most depleted lavas (dredges 8a, 28, 29a) may represent normal oceanic crust (Werner *et al.*, 2003). In contrast, 26-TVG-1 displays a relatively flat rare earth element (REE) pattern, similar to those from samples collected to its south on the PLUME02 cruise (Harpp & White, 2001), and is consequently considered as part of the Carnegie Ridge despite its location on the northern flanks. In general, there is a broad trend of increasing enrichment in incompatible trace elements (ITE) and radiogenic isotope signatures eastward along the ridge.

The Cocos Ridge

Cocos Ridge axis (dredges 35, 37, 39, 43–45, 49–55). Lavas collected from the Cocos Ridge axis are all tholeiitic basalts with MgO ranging from 2·90 to 11·61 wt % (Werner *et al.*, 2003). Limited radiogenic isotope analyses from six samples exhibit less variation than is observed on the Carnegie Ridge (ε_{Nd} 6·01–7·74; Werner *et al.*, 2003). Dredge 29a sampled the ocean floor at the 91°W transform fault on the GSC, revealing a tholeiitic basalt (MgO 8·52 wt %) that is slightly more depleted (ε_{Nd} 7·56; Werner *et al.*, 2003) than lavas erupted along the GSC axis both to the east and west of the fracture zone (Schilling *et al.*, 1982; Detrick *et al.*, 2002).

Cocos Ridge axial samples exhibit a similar range in trace element contents to those from the Carnegie Ridge, but extend to more enriched ITE ratios (Figs 3–5). Lavas with the steepest REE patterns also have the most pronounced negative Eu anomalies (e.g. dredges 51, 53; Fig. 3), corresponding to the greatest modal abundance of plagioclase phenocrysts (25–30%). The depleted lavas are not typical N-MORB, but broadly resemble those of the southern Carnegie Ridge flanks (Harpp & White, 2001) and Genovesa Island (Harpp *et al.*, 2002), with concave-down REE patterns (Fig. 3). Similar to the Carnegie Ridge, Cocos Ridge lavas become increasingly enriched in ITE and radiogenic isotope ratios eastward along the axis.

Costa Rica Seamount Province (dredges 46–48, 56, 58–63, 73–87). Lavas from the Costa Rica Seamount Province are both tholeiitic and alkalic, with a large range of differentiation (Table 3; MgO 1·93–8·04 wt %). Radiogenic isotope signatures are slightly more enriched than those along the Cocos Ridge axis (ε_{Nd} 3·90–6·63; Werner *et al.*, 2003). All the Costa Rica Province lavas are highly enriched in ITE, displaying steeply dipping REE patterns (Fig. 3; Hoernle *et al.*, 2000).

Seamounts in the center of the Costa Rica Seamount Province have elevated $(La/Sm)_n$ ratios compared with those on the outskirts, and lavas at the northern periphery are the most depleted of the region. The lavas with the shallower heavy REE slopes are found on the western and eastern edges of the province.

Cocos Island Province (dredges 38, 40–42, 64–72, Cocos Island). Cocos Province lavas are alkalic, with a wide range of MgO contents (0·48–8·83 wt %; Werner *et al.*, 2003). The lavas define coherent trends in major element diagrams, consistent with clinopyroxene fractionation (i.e. positive Sc/Y and CaO/Al_2O_3 vs MgO slopes). Isotopic compositions (ε_{Nd} 5·77–7·41; Werner *et al.*, 2003) suggest that the Cocos Province lavas are derived from a relatively enriched mantle source; Cocos Island lavas have a limited range in isotopic ratios (ε_{Nd} 6·34–6·83; Werner *et al.*, 2003), as first noted by Castillo *et al.* (1988).

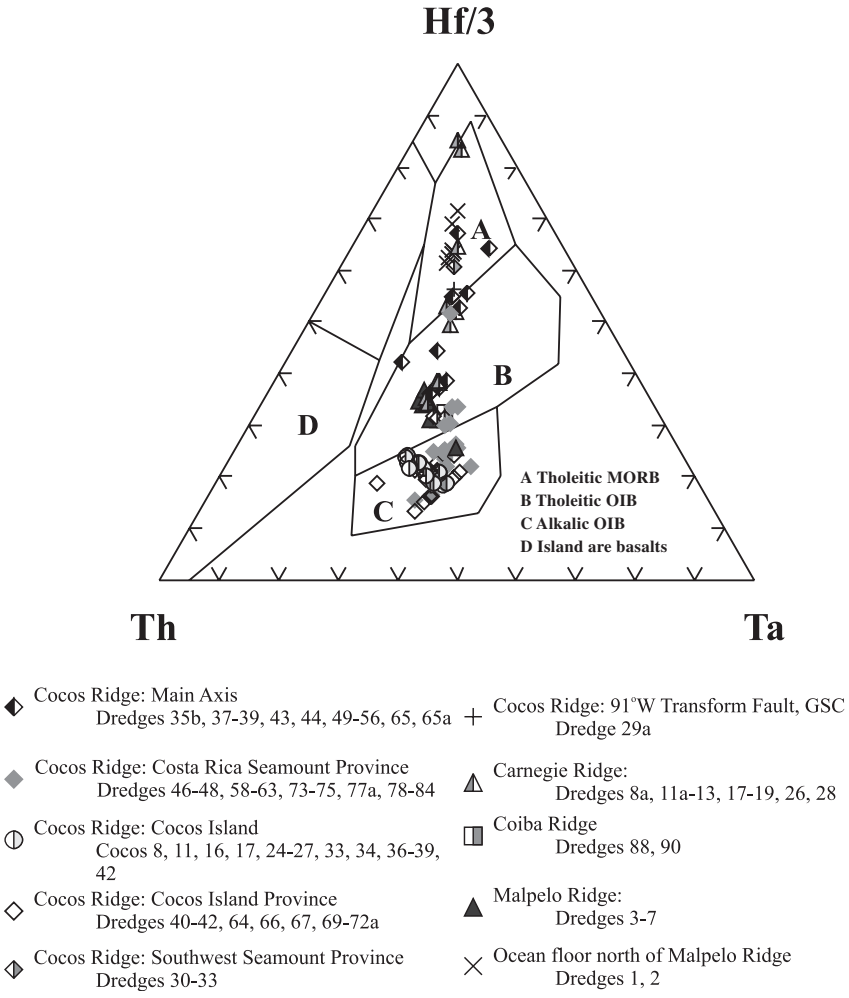

Fig. 2. Th–Hf–Ta discrimination diagram for aseismic ridge basalts, from Wood (1980).

Cocos Island and the nearby seamounts are highly enriched in incompatible trace elements (Figs 3–5). Some lavas exhibit a distinctive concave-up REE pattern, with steep slopes in the light REE (LREE) but nearly horizontal slopes in the heavy REE (HREE), causing some of the patterns to cross (Fig. 3), reminiscent of Floreana Island and SW Galápagos seamount lavas (White *et al.*, 1993; Harpp & White, 2001); the spoon-shaped patterns are observed most strongly in the submarine lavas.

Interestingly, lavas from dredge 38, located over 150 km east of Cocos Island, display the same enriched compositions as the Cocos Island Province. Sample 39-DR-2, however, collected from a seamount approximately midway between dredge 38 and Cocos Island (Fig. 1), has a nearly flat REE pattern (Fig. 3) and bears little resemblance to the Cocos Province lavas.

Southwest Seamount Province (dredges 30–33)

The Southwest Seamount Province consists of tholeiitic basalts with a large range in MgO content (4·62–10·17 wt % for four samples; Werner *et al.*, 2003) but little variation in isotopic composition (ε_{Nd} 5·95 and 6·28; Table 3; Werner *et al.*, 2003). The Southwest Province lavas vary from LREE-enriched to LREE-depleted, but never achieve the enrichment of the Costa Rica or Cocos Island Province lavas (Fig. 3).

The Coiba Ridge (dredges 88, 90)

Both of the Coiba Ridge lavas are tholeiitic basalts (MgO 5·19–5·56 wt %; Table 3) enriched in ITE (Fig. 2), like the more depleted of the Costa Rica seamounts and the most enriched lavas from the main Cocos Ridge axis (Figs 3 and 4).

The Malpelo Ridge (dredges 1–7)

The Malpelo Ridge lavas (dredges 3–7) are all plagioclase-phyric, tholeiitic basalts, except for 6-DR-1, which is alkalic. The major element compositions (MgO 4·68–7·75 wt %) resemble those of the more primitive Costa

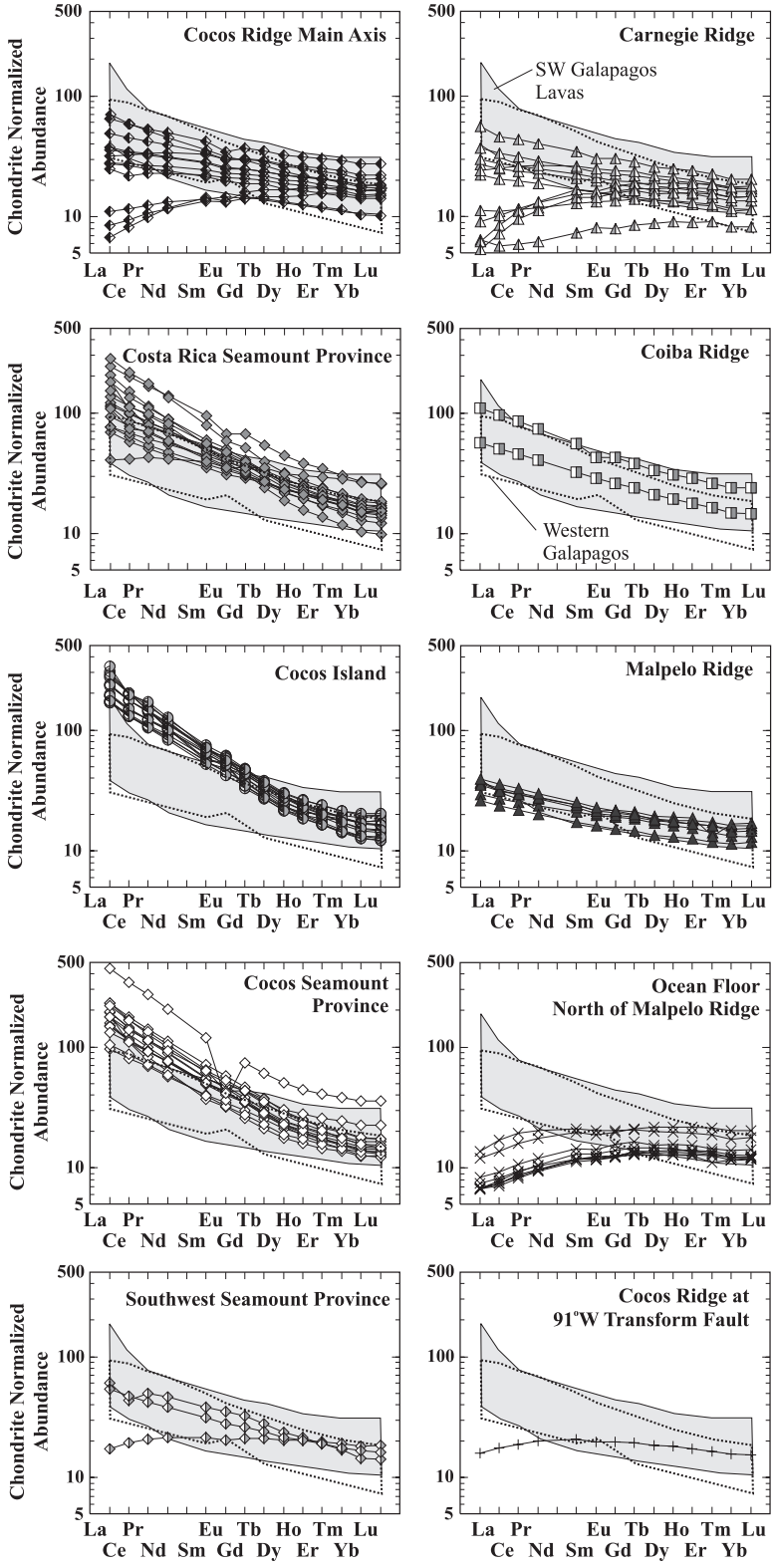

Fig. 3. Rare earth element concentrations by region. Symbols as in Fig. 2. Chondrite normalization values from Sun & McDonough (1989). All data are shown, including samples with evidence of seawater alteration (see text for details). Light grey field shows lavas from the SW Galápagos including Floreana Island (White *et al.*, 1993; Harpp & White, 2001); field with dotted outline represents lavas from Fernandina Island, Western Galápagos (White *et al.*, 1993; Kurz & Geist, 1999).

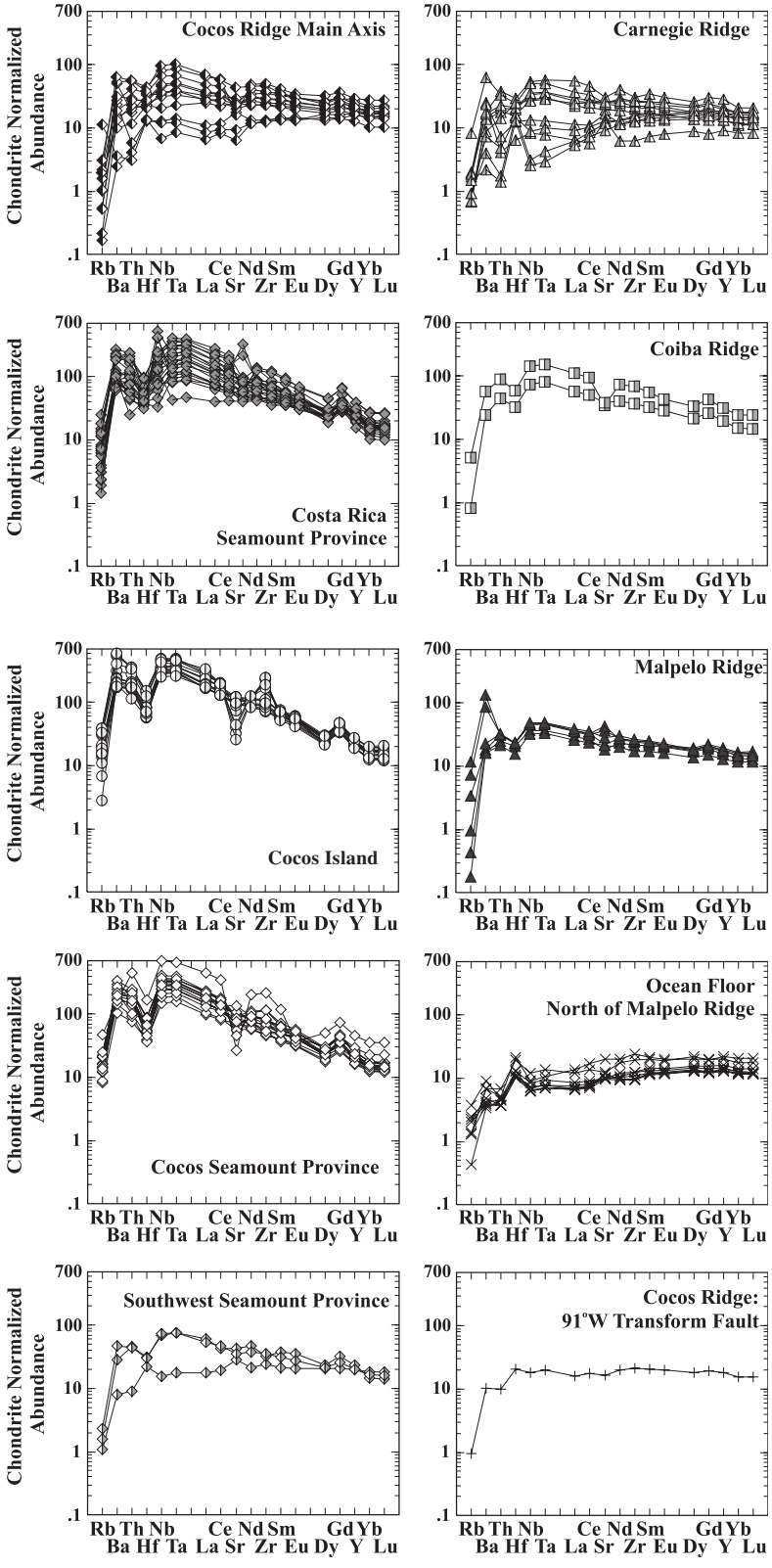

Fig. 4. Trace element concentrations by region. Symbols as in Fig. 2. Order of elements and chondrite normalization values from Sun & McDonough (1989). All data are shown, including samples with evidence of seawater alteration; in all subsequent figures, the altered samples have been removed from consideration (see text for details).

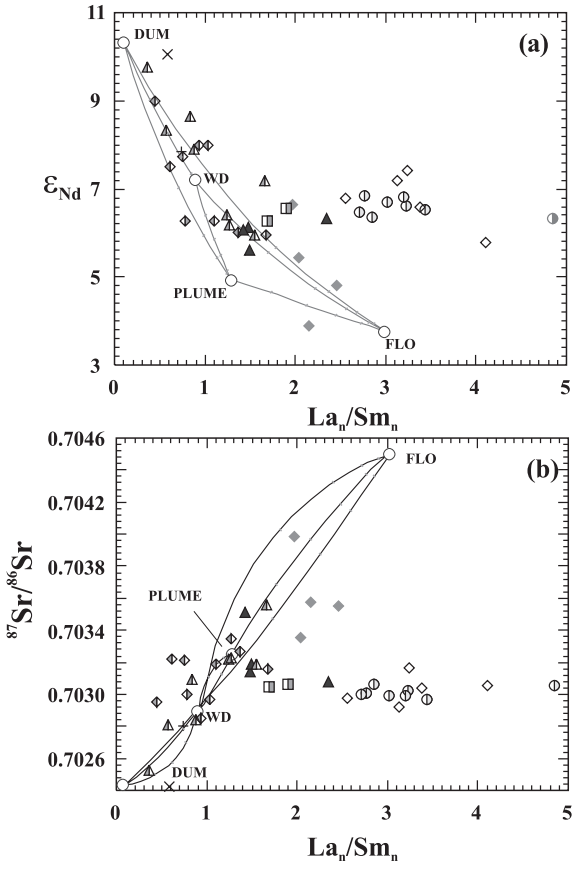

Fig. 5. Variation of incompatible trace element ratios with radiogenic isotope ratios from Werner *et al.* (2003). (a) $(La/Sm)_n$ vs ε_{Nd}; (b) $(La/Sm)_n$ vs $^{87}Sr/^{86}Sr$. Symbols as in Fig. 2. ○, Proposed mantle end-member compositions of Harpp & White (2001). PLUME, 'pristine' plume; DUM, depleted upper mantle; FLO, incompatible element enriched material; WD, component distinctive primarily in its Pb isotopes. Bold grey lines are mixing curves between pairs of end-members, calculated using the approach of Langmuir *et al.* (1978). Tick marks on mixing curves represent 20% divisions (i.e. mark closest to an end-member represents 80% of that end-member plus 20% from the other).

Rica Seamount Province lavas, with moderately well-correlated major oxide variations and a narrow isotopic range (ε_{Nd} 5·62–6·34; Werner *et al.*, 2003). Malpelo Ridge lavas exhibit uniformly ITE-enriched compositions, similar to those observed on the Coiba Ridge and the Cocos Ridge axis, but with gentler slopes in the HREE and lower absolute concentrations on average.

Lavas dredged from an abandoned spreading center north of the Malpelo Ridge (dredges 1 and 2) are tholeiitic (MgO 5·70–8·72 wt %) and distinctly more depleted (ε_{Nd} 10·05; Figs 3–5; Werner *et al.*, 2003) than those from the main Malpelo Ridge. Their location and composition suggest that these lavas are probably normal oceanic crust rather than the products of hotspot activity.

DISCUSSION

Heterogeneous mantle sources

In a statistical analysis of regional Galápagos compositions, Harpp & White (2001) proposed that the complex isotopic and trace element variations observed throughout the archipelago are the result of interaction between four mantle source reservoirs with distinct radiogenic isotope ratio signatures (Table 4): (1) a mantle plume with relatively enriched compositions (PLUME); (2) the depleted upper mantle (DUM); (3) an incompatible element-enriched, possibly metasomatically altered reservoir (FLO), which may or may not be part of the Galápagos plume (e.g. Kurz & Geist, 1999; Blichert-Toft & White, 2001); (4) a fourth component distinctive primarily in its lead isotope ratios (WD; elevated $^{207}Pb/^{204}Pb$ and $^{208}Pb/^{204}Pb$ for a given $^{206}Pb/^{204}Pb$).

Radiogenic isotope ratios

The compositions of the four mantle end-members interacting in the Galápagos emerged from principal component analysis (PCA) of radiogenic isotope ratios in Galápagos lavas (Harpp & White, 2001). Principal component analysis is a multivariate statistical method designed to reduce the complexity of a dataset by transforming the original, observed variables (in this case, isotopic ratios and later trace element ratios) into a new set of variables called principal components. The new variables are vectors that consist of different linear combinations of the original geochemical data. The first principal component vector accounts for as much of the variance in the dataset as possible; the second does the same for the remaining variability, and so forth. The extent to which the principal component represents the original dataset is indicated by the eigenvalue, or variance proportion. Effectively, PCA provides a method for reducing a multivariate system to a more manageable number of dimensions, without making any assumptions about the original data. The distribution of the variance across the principal component vectors indicates the number of variables necessary to describe the dataset efficiently. For example, when the majority of the variance is taken into account by the first principal component vector, the data can be described in one-dimensional space by two end-member compositions without any significant loss of information. Similarly, if two eigenvectors share the bulk of the variance, three end-member compositions adequately represent the original dataset's variability.

For the Galápagos archipelago dataset, we normalized all of the isotopic ratios to their mean prior to calculating the PCA results, because their values differ by orders of magnitude; in this way, all geochemical observations are afforded equal weight in the analysis. When only the

Table 3: Regional characteristics of dredged lavas

Sample	Location	Composition	Regional ε_{Nd} range*	Regional $^{87}Sr/^{86}Sr$ range*	Trace element characteristics $(La/Sm)_n$	Trace element characteristics $(Sm/Yb)_n$	Melting model results	Dominant melt generation field
Cocos Island Province			**6·33—7·41**	**0·702924—0·703163**	**2·30—4·86**	**2·83—4·44**		
Cocos *8*, 11, *16*, *17*, *24*, 25, 26, *27*, 33, 34, 36, 37, 38, *39*, *42*	Cocos Island	Alkalic	6·33—6·83	0·702972—0·703063	2·71—4·86	2·98—4·44	<1% PLUME	garnet
38-DR-12	Mid-Cocos Ridge axis, E flank	Alkalic	5·77	0·703059	4·10	2·92	<1% PLUME	garnet
65-DR-12, 65a-DR-1	NE Cocos Ridge, E flank	Alkalic			3·37—3·58	3·38—3·56	<1% PLUME	garnet
40a-DR-1, 41-DR-1, 42-DR-1, *64a-DR-1*, 64-DR-1, 66-DR-1, 67-DR-1, 69-DR-1, 70b-DR-1, 71a-DR-1, 71-DR-1, 72a-DR-1	Cocos Island Prov., Cocos Ridge	Alkalic	6·59—7·41	0·702924—0·703163	2·30—3·58	2·83—3·99	<1% PLUME	garnet
Costa Rica Seamount Province			**3·90—6·63**	**0·703359—0·703982**	**0·99—3·60**	**1·47—4·48**		
46-TVG-1, 47-DR-1, 48-DR-1, 58a-DR-1, 60-DR-1, 62-DR-1, 63a-DR-1, *77-DR-1*, 78-DR-1, 79-DR-7, 80-DR-1, 81-DR-1, *82-DR-1*, 83-DR-1, 84-DR-2	Costa Rica Seamount Prov., Cocos Ridge	Alkalic	3·90—5·44	0·703359—0·703572	1·67—3·60	2·22—4·48	0·5—2% PLUME + FLO	garnet
56-TVG-1, *73-DR-1*, 74-DR-1, *75-DR-1*, 77a-DR-1, 85-DR-1	Costa Rica Seamount Prov., Cocos Ridge	Tholeiitic	6·63 (74-DR-1)	0·703982 (74-DR-1)	0·99—2·00	1·47—2·24	5—10% PLUME +FLO (+WD? in 74, 78)	garnet
SW Seamount Province								
30-DR-9, 32-DR-1, 33-DR-1	SW Seamount Prov., Cocos Ridge	Tholeiitic	5·95—6·28	0·702999—0·703161	0·78—1·68	1·17—2·60	2—>5% PLUME (+DUM)	garnet
Cocos Ridge axis			**5·77—8·00**	**0·702852—0·703269**	**0·61—4·10**	**0·90—3·56**		
35b-DR-1, *39 DR-2*	Mid-Cocos Ridge axis	Tholeiitic	7·74 (35b-DR-1)	0·703212 (35b-DR-1)	0·76—1·03	1·33—1·93	2—10% PLUME (+DUM)	garnet
43-DR-1	Mid-Cocos Ridge axis, E flank	Tholeiitic	8·00	0·702852	0·94	1·45	2—10% PLUME (+DUM)	garnet
44-DR-14, 50-DR-1, 51-DR-1, 52-DR-1	NE Cocos Ridge, E flank	Tholeiitic	7·53 (44-DR-14)	0·703219 (44-DR-14)	0·61—1·47	0·90—1·50	2—10% PLUME (+DUM)	garnet
49a-DR-1, 53-DR-1, 54a-DR-1, 55-DR-1	NE Cocos Ridge axis	Tholeiitic	6·05—6·28	0·703188—0·703269	1·09—1·87	1·46—2·01	2—10% PLUME (DUM)	garnet
Cocos Plate ocean floor			**7·86—8·99**	**0·702803—0·702954**	**0·45—0·74**	**0·86—1·30**		
29a-DR-5	Ocean floor at 91°W transform	Tholeiitic	7·86	0·702803	0·74	1·30	>10% PLUME +DUM	garnet
37-DR-1	Ocean floor S of Cocos Ridge	Tholeiitic	8·99	0·702954	0·45	0·86	>10% PLUME +DUM	garnet
Nazca Plate ocean floor								
8a-DR-1, 8a-DR-5, 26-TVG-1	Ocean floor N of Carnegie Ridge	Tholeiitic	7·90—9·77	0·702530—0·702842	0·36—0·88	0·92—1·48	>10% melting DUM (+PLUME)	garnet

Table 3: continued

Sample	Location	Composition	Regional ε_{Nd} range*	Regional $^{87}Sr/^{86}Sr$ range*	Trace element characteristics $(La/Sm)_n$	Trace element characteristics $(Sm/Yb)_n$	Melting model results	Dominant melt generation field
Malpelo Ridge			**5·74—10·05**	**0·702424—0·703514**	**0·50—2·34**	**0·90—3·00**		
3-TVG-4, *5-DR-1, 5-DR-11*, 5-DR-21, 5-DR-26, 6-DR-1, 6-DR-4, 7-DR-1	Malpelo Ridge	Tholeiitic	5·74—6·34	0·703081—0·703514	1·34—2·34	1·40—3·00	2—>5% melting PLUME (+DUM)	garnet
1-DR-1, 1-DR-15, 1-DR-16, 1-DR-17, 1-DR-18, 1-DR-19, 2-DR-1, 2-DR-1a	Ocean floor near Coiba, Malpelo	Tholeiitic	10·05 (2-DR-1)	0·702424 (2-DR-1)	0·50—0·63	0·90—1·19	>10% melting PLUME + DUM	garnet
Carnegie Ridge axis			**6·18—8·66**	**0·702813—0·703557**	**0·57—1·55**	**0·75—1·66**		
11a-DR-1 m 11a-DR-19, 12-DR-1, 13-DR-1	E Carnegie Ridge	Tholeiitic	6·18—6·40	0·703225—0·703227	1·24—1·55	1·48—1·66	>1—5% PLUME (+minor DUM)	garnet
19-DR-4, 28-DR-1	S Carnegie Ridge	Tholeiitic	8·35 (28-DR-1)	0·702813 (28-DR-1)	0·57—0·85	0·86—0·94	2—>5% PLUME (+DUM)	garnet
17-TVG-1	SE Carnegie Ridge	Alkalic	7·20	0·703557	1·66	0·75	2—>5% PLUME (+DUM, minor FLO)	garnet
17-TVG-3, 18-DR-1	SE Carnegie Ridge	Tholeiitic	8·66 (18-DR-1)	0·703094 (18-DR-1)	0·83—1·41	1·09—1·46	2—>5% PLUME (+DUM, minor FLO)	garnet
Coiba Ridge								
88-DR-1, 90-DR-8	Coiba Ridge	Tholeiitic	6·26—6·57	0·703049—0·703067	1·68—1·90	2·12—2·25	1—2% PLUME	garnet

*From Werner *et al*. (2003).

Ranges shown in bold type for each broad geographical area are summaries for the entire region, including all subdivisions listed below it; where there are no subdivisions within the geographical area, no summary is included in the table. The melting model results column indicates the fraction of melting (in %) of a mantle source necessary to generate the observed lava compositions in each area. PLUME, DUM, FLO and WD are the Harpp & White (2001) mantle end-member compositions used as the mantle source starting composition. For instance, '2—5% PLUME' means that 2—5% melting of a PLUME mantle source is capable of generating the compositions of the lavas being modeled. Samples with significant seawater alteration and the most highly differentiated Cocos Island rocks (MgO <5·0 wt %) have been excluded from all subsequent discussion; they are shown in italics here. Ranges in Sr isotopic ratios are sometimes significantly greater than those for ε_{Nd} for the same samples; this is probably the result of seawater alteration that has elevated the $^{87}Sr/^{86}Sr$ of the lavas, despite leaching carried out prior to analysis to eliminate such effects (Werner *et al*., 2003).

Table 4: Proposed mantle end-member compositions in the Galápagos archipelago

End-member	$^{87}Sr/^{86}Sr$	$^{143}Nd/^{144}Nd$	ε_{Nd}	$^{206}Pb/^{204}Pb$	$^{207}Pb/^{204}Pb$	$^{208}Pb/^{204}Pb$	$^{3}He/^{4}He$	Ba/La	$(La/Sm)_n$
FLO	0·70450	0·51283	3·8	21·2	15·77	41·0	3	35	3·0
PLUME	0·70328	0·51289	5·0	18·9	15·49	38·3	32	5	1·3
WD	0·70290	0·51301	7·2	19·3	15·67	39·5	9	8	0·9
DUM	0·70243	0·51317	10·4	18·1	15·46	37·5	8	1	0·1

End-member compositions were determined using principal component analysis of the entire Galápagos archipelago dataset [submarine and subaerial lavas; see text and Harpp & White (2001)] using all the isotopic ratio parameters listed in the table. The first three eigenvectors account for 70·9%, 20·6% and 5·5% of the total variance in the dataset, respectively. These results suggest that four mantle reservoirs with distinct compositions must be interacting to explain the observed geochemical variations in the Galápagos archipelago. The Ba/La and $(La/Sm)_n$ values were estimated based on subsequent mixing calculations (Harpp & White, 2001).

isotopic ratios are considered for all subaerial and submarine data available in the present-day Galápagos archipelago, the first two eigenvectors (e1 + e2) account for 94·3% of the variance and the first three explain 97·3% (Table 5a; Harpp & White, 2001). Based on these results, Harpp & White (2001) concluded that three or four compositionally distinct mantle end-members must be interacting in the region to explain the observed isotopic variations.

When the isotopic ratios from the Cocos and Carnegie Ridges are included in the calculations with the Harpp & White (2001) dataset (i.e. all available submarine and subaerial isotopic analyses from the Galápagos archipelago), the PCA result does not change significantly (Table 5b; e1 + e2 = 93·5%; e1 + e2 + e3 = 97·2%). The eigenvectors are not dominated by any single isotopic ratio, consistent with the results from the archipelago lavas alone. These statistical calculations confirm the conclusion of Hoernle *et al.* (2000) and Werner *et al.* (2003) that the lavas of the Cocos, Carnegie, Malpelo, and Coiba Ridges are derived from the same mantle source materials as <3 Ma Galápagos archipelago lavas. Thus, the Galápagos plume has probably maintained its distinctive compositional heterogeneity for the past ~20 Myr.

Incompatible trace element ratios

To date, conclusions about the longevity of the chemical zonation in the Galápagos plume have been based exclusively on radiogenic isotope analyses. Because the geochemical variations are probably the result of mixing between different mantle reservoirs (White *et al.*, 1993; Blichert-Toft & White, 2001; Harpp & White, 2001), the compositional heterogeneity should be reflected in elemental concentrations as well, particularly ratios of incompatible trace elements that can serve as tracers of mantle sources.

Furthermore, Harpp & White (2001) found that ITE ratios were consistent with their model involving variable contributions of four mantle sources for the present-day Galápagos plume (Table 4). The aseismic ridge samples fall within the limits defined by the four Galápagos archipelago mantle components (Harpp & White, 2001; Fig. 5). To test this conclusion statistically, we added aseismic ridge data for Ba/La, La/Ce, La/Nb, Th/U, Y/Gd, and Sm/Zr to the isotopic dataset tested in the previous PCA. The elements used in the ratios were chosen on the basis of similar distributions in mantle reservoirs (Sun & McDonough, 1989), as well as broadly similar partition coefficients for clinopyroxene (GERM website).

Inclusion of the ITE ratios from the aseismic ridges with the archipelago isotopic dataset has a profound effect on the PCA results (Table 5c). The first two eigenvectors account for only 77·8% of the variance, and the first three explain nearly 10% less of the variance than they do in the equivalent dataset for young Galápagos lavas (e1 + e2 + e3 = 87·9%).

Whereas radiogenic isotope ratios are unaffected by melting and crystallization processes, making them ideal tracers of mantle source compositions, even the carefully chosen ITE ratios used in the PCA can be affected by differences in melt generation conditions and, to a lesser extent, crustal contamination. Taken together, the statistical results suggest the following fundamental conclusions: first, the heterogeneous mantle source(s) responsible for the variation observed in the Galápagos archipelago is the same as that for the seamounts along the aseismic ridges, as predicted by Hoernle *et al.* (2000) and supported by Werner *et al.* (2003). Second, PCA results that indicate decoupling between the isotopic and ITE ratios imply that the conditions responsible for melt generation in the aseismic ridge lavas differ, at least in part, from those affecting the present-day Galápagos archipelago.

Both the Galápagos archipelago and the aseismic ridges exhibit similar ranges in isotopic and ITE ratios. The lavas with the most extreme isotopic enrichment in

Table 5: Principal component analysis results summary

(a) Galápagos archipelago data: isotopic ratios only (from Harpp & White, 2001)

	Variance proportion				
Eigenvectors	V1	V2	V3	V4	V5
% of total	84·7	9·6	3·3	2·1	0·3
$^{87}Sr/^{86}Sr$	0·435	0·474	0·693	0·325	0·016
ε_{Nd}	0·433	0·498	0·710	0·214	0·126
$^{206}Pb/^{204}Pb$	0·470	0·063	0·104	0·736	0·471
$^{207}Pb/^{204}Pb$	0·419	0·691	0·023	0·511	0·293
$^{208}Pb/^{204}Pb$	0·477	0·216	0·070	0·213	0·822

(b) Cocos and Carnegie Seamount data: isotopic ratios only

	Variance proportion				
Eigenvectors	V1	V2	V3	V4	V5
% of total	84·5	9·0	3·7	2·4	0·4
$^{87}Sr/^{86}Sr$	−0·428	−0·545	−0·683	−0·221	0·067
ε_{Nd}	0·431	0·503	−0·726	0·134	−0·125
$^{206}Pb/^{204}Pb$	−0·464	0·200	−0·071	0·751	0·419
$^{207}Pb/^{204}Pb$	−0·432	0·610	0·005	−0·594	0·296
$^{208}Pb/^{204}Pb$	−0·478	0·195	0·020	0·127	−0·847

(c) Cocos and Carnegie Seamount data: isotopic and incompatible trace element ratios

	Variance proportion							
Eigenvectors	V1	V2	V3	V4	V5	V6	V7	V8
% of total	64·6	13·2	10·1	5·5	3·7	1·7	1·0	0·3
$^{87}Sr/^{86}Sr$	0·352	−0·300	0·174	−0·663	0·231	0·464	−0·212	−0·045
ε_{Nd}	−0·396	0·169	0·188	0·359	0·174	0·588	−0·444	0·279
$^{206}Pb/^{204}Pb$	0·406	−0·117	−0·052	0·372	0·304	−0·300	−0·619	−0·339
$^{207}Pb/^{204}Pb$	0·398	−0·128	−0·032	0·490	0·076	0·501	0·514	−0·251
$^{208}Pb/^{204}Pb$	0·430	−0·033	−0·090	0·109	0·218	−0·149	0·076	0·848
Ba/La	0·200	0·497	0·805	−0·014	0·125	−0·159	0·136	−0·067
La_n/Ce_n	0·381	0·163	0·025	0·045	−0·840	0·165	−0·293	0·081
Th/U	0·163	0·759	−0·523	−0·197	0·220	0·153	−0·017	−0·111

Results are similar for all combinations of ITE ratios listed in the text; only a representative selection is shown here. The important result here is that when the ITE ratios from the aseismic ridges are included with the Galápagos archipelago data for a PCA, the variance explained by the first three eigenvectors is nearly 10% less than for the isotopic data alone. This suggests that the ITE and isotopic ratios are controlled by different processes. Isotopic ratio variations are probably the result of a consistent (but heterogeneous) mantle source common to the present-day archipelago and the aseismic ridges. In contrast, ITE ratios may be the result of differences in melt generation processes at the hotspot center compared with those along the aseismic ridges.

the archipelago (Floreana and the SW Galápagos Platform) also possess the most extreme ITE ratios, and are thought to be the result of low-degree melts generated in the spinel peridotite facies (Fig. 5; White *et al.*, 1993; Harpp & White, 2001). In contrast, aseismic ridge lavas from this dataset showing the greatest degree of isotopic enrichment (Costa Rica Seamount Province, Carnegie, and Malpelo Ridges) are not those with the most extreme ITE ratios (Fig. 5; Cocos Island Province). This observation suggests that segments of the aseismic ridges have experienced different melting conditions from those affecting the Galápagos archipelago, although nevertheless sharing the same compositionally heterogeneous mantle source(s).

Spatial trends in melt generation across the aseismic ridges

Harpp & White (2001) used isotopic ratios (Sr, Nd, and Pb) to define relative contributions of the four mantle end-members to every Galápagos lava. The resulting source mixture was then melted using a polybaric melt model of trace element ratios (La/Sm and Sm/Yb; Fig. 6). We have applied the results of this model to the REE of the aseismic ridge lavas in regional groups to determine plausible ranges for end-member contributions and approximate melting conditions (Figs 5 and 6; Table 3).

The Carnegie and Malpelo Ridges (dredges 1–8, 11a–13, 17–19, 26, 28, 29a)

Lavas from the main Carnegie Ridge (dredges 11–13) exhibit dominantly PLUME-like compositions, with some contribution from DUM, and are consistent with >1–5% melting of their mantle source, at least partially in the garnet stability field (Harpp & White, 2001). These lavas are nearly indistinguishable from those erupted more recently in the central Galápagos archipelago (White *et al.*, 1993; Harpp & White, 2001). Lavas from the Malpelo Ridge exhibit similar characteristics (Fig. 6a).

Lavas from the ridges' flanks (dredges 1, 2, 8a, 26, 28, 29a) appear to be derived from >10% melting of a more depleted mantle source. The southern ridge flank lavas (dredges 17–19) resemble those dredged during the PLUME02 cruise on the southern periphery of the Galápagos platform (Christie *et al.*, 1992; Harpp & White, 2001), and are derived from a more PLUME-enriched source than those from the north flank, as indicated by the isotopic data (Werner *et al.*, 2003). The southern Carnegie Ridge lavas may incorporate a minor contribution from the FLO end-member, manifested in the isotopic ratio–ITE ratio plot as an array offset toward the enriched FLO composition (Fig. 5).

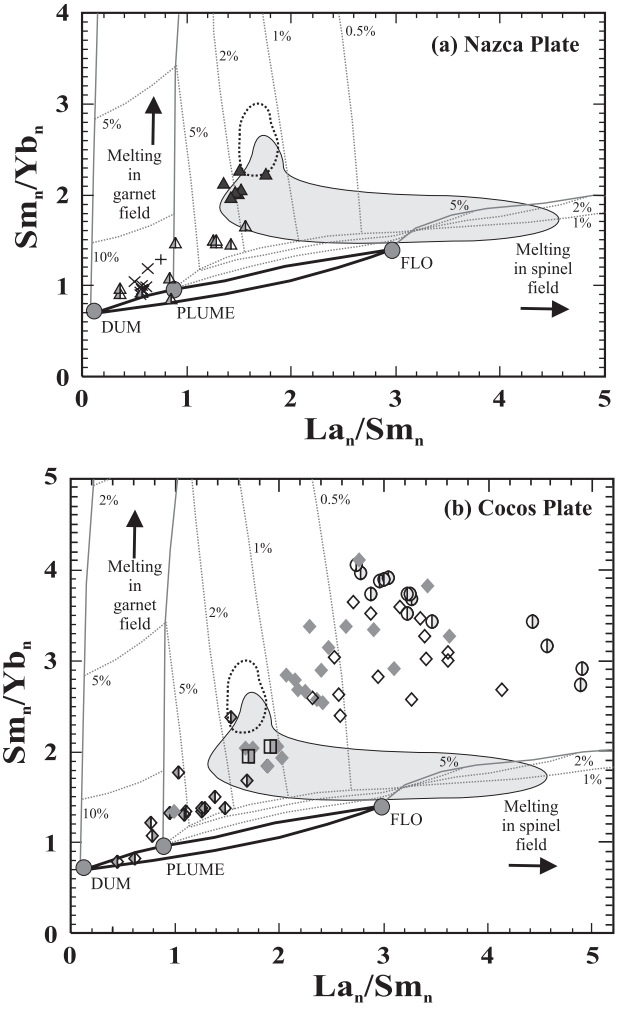

Fig. 6. Measured REE ratios of aseismic ridge lavas compared with predicted values for the polybaric melt model of Harpp & White (2001) based on interactions among three mantle end-members, DUM, PLUME, and FLO. Bold black lines represent mixing between pairs of mantle sources. The WD end-member is not included in this diagram because it is distinct only in its Pb isotopic ratios. In the melt model, mixtures of end-members are melted to varying extents in either the spinel or garnet stability fields of the mantle (>60–80 km for the garnet stability field and ~60–25 km for spinel). Specifically, an ascending parcel of mantle undergoes equilibrium melting according to the melt function of Langmuir *et al.* (1992; ~1·2% melting/kbar of upwelling) and the algorithm developed by Gallahan & Nielsen (1992) for the compositional dependence of REE partition coefficients in clinopyroxene. Liquid is then partially extracted and pooled, and the remaining residue is used as the source for each subsequent melt increment. Consequently, the pooled melt has an aggregate composition that reflects the average pressure and temperature of the melting interval (Harpp & White, 2001). Melts of pure DUM and PLUME in the garnet stability field are indicated in the figure; PLUME and FLO melts are generated in the spinel stability field as labeled. Numerals represent extent of melting (%). Aseismic ridge lava symbols as in Fig. 2. (a) Lavas collected from the Carnegie and Malpelo Ridges; (b) lavas collected from the Cocos and Coiba Ridges. Grey field shows lavas from the SW Galápagos including Floreana Island (White *et al.*, 1993; Harpp & White, 2001); field with dashed outline shows lavas from Fernandina Island, Western Galápagos (White *et al.*, 1993; Kurz & Geist, 1999).

The Cocos Ridge axis and Coiba Ridge (dredges 35, 37, 39, 43–45, 49–55, 88, 90)

Compositions of Cocos axial lavas and those from the Coiba Ridge substantially overlap those of the Carnegie Ridge (Fig. 6b). The melt model indicates that lavas from the axis of the Cocos Ridge are primarily the result of ~2–10% melting of a PLUME source, with the exception of the samples that appear to be normal MORB (e.g. dredges 37, 44). Most of the Cocos axis samples resemble lavas erupted in the western Galápagos archipelago, in that their sources are PLUME-dominated but diluted by depleted mantle (Fig. 5). Coiba Ridge lavas are produced from lower degrees of melting (Fig. 6b) of a more pristine PLUME source (1–2%).

Costa Rica Seamount Province (dredges 46–48, 56, 58–63, 73–87)

Most of the lavas from the Costa Rica Seamount Province (Fig. 6b) appear to be derived from a source that is predominantly PLUME, with small, variable contributions from FLO and some WD. The lavas with the most prominent WD signatures are located at the western edge of the province (dredges 74 and 78; determined from Pb isotopic ratios, not shown here). Most of the Costa Rica seamounts are compositionally similar to lavas from the SW corner of the Galápagos archipelago, near Cerro Azul on Isabela Island (White *et al.*, 1993; Harpp & White, 2001). An important feature distinguishes the bulk of the Costa Rica seamounts from the SW Galápagos Platform lavas; the Costa Rica seamount lavas have elevated $(Sm/Yb)_n$ ratios in addition to high $(La/Sm)_n$. These REE systematics suggest that the Costa Rica Province is the product of low degrees of melting (<2%) of a PLUME + FLO source, mostly in the garnet stability field. No lavas dominantly derived from PLUME in the present Galápagos exhibit comparable REE systematics. Lavas from the seamounts at the outer edges of the province are products of greater extents of melting (5–10%; dredges 56, 73–75, 77a; Fig. 6b).

Cocos Island Province (dredges 38, 40–42, 64–72, Cocos Island)

Cocos Island and the Cocos Province seamounts exhibit many similar characteristics to the Costa Rica Seamount Province, except that Cocos Island and some of the seamounts extend to higher $(La/Sm)_n$ and $(Sm/Yb)_n$ (Table 3; Fig. 6b). They are also distinct from lavas observed in the present-day Galápagos because of their extreme ITE ratios coupled with PLUME-like isotopic signatures. These characteristics suggest that the lavas of Cocos Island and the surrounding seamounts are derived from a predominantly PLUME-like source that has experienced low extents of melting (<1%) in the garnet stability field and considerable subsequent fractional crystallization.

Southwest Seamount Province (dredges 30–33)

Although data are sparse in this region, the SW seamounts appear to be derived from a PLUME + DUM mantle source, similar to that for most of the Cocos Ridge lavas (Fig. 6b). The SW seamounts are the products of moderate (2–>5%) extents of melting, probably in the garnet facies. If WD contributes to this set of lavas, it is only to a minor extent, unlike the northern Galápagos lavas across the GSC.

Tectonic implications for melt generation and plume–ridge interaction

Tectonic history of the Galápagos plume–GSC system

In their isotopic study of the aseismic ridge lavas, Werner *et al.* (2003) proposed that the Galápagos plume has maintained its compositional zonation for the past ~20 Myr. Although they confirmed the striped zonation along the NE Cocos Plate hotspot track, the southwestern part of the track does not exhibit the same pattern, a result of the young age of the samples collected on the SW Cocos Ridge (Werner *et al.*, 2003). They explained deviations from the predicted pattern with a tectonic model for the region that takes into account plate reconstructions (e.g. Wilson & Hey, 1995; Meschede & Barckhausen, 2000; Barckhausen *et al.*, 2001), the changing relationship between the migrating GSC and the Galápagos hotspot, including the relatively recent formation of the 91°W transform fault and a pre-existing large-offset transform (Wilson & Hey, 1995; Meschede & Barckhausen 2000), and variations in the morphology of the volcanic structures along the hotspot track.

Briefly, Werner *et al.* (2003) proposed the following sequence of events: (1) the GSC initiated a southward jump to the northern edge of the Galápagos hotspot at 19·5 Ma; (2) from 19·5 to 14·5 Ma, the GSC was centered above the hotspot, erupting plume material onto both the Cocos and Nazca Plates; (3) at 14·5 Ma, a second ridge jump relocated the GSC south of the hotspot, such that the majority of the plume products were erupted onto the Cocos Plate; (4) between 11 and 12 Ma, the plume was centered beneath an offset along the GSC, when (5) at 4 Ma, the GSC relocated north of the hotspot, leaving the plume isolated beneath the Nazca Plate, as is the case today. Currently, the northeastward migration of the GSC continues, increasing the distance between the spreading center and the hotspot (e.g. Wilson & Hey, 1995).

Whereas the Werner *et al.* (2003) model is consistent with the distribution of isotopic signatures observed along the aseismic ridges and with changes in ridge volume over time, it does not adequately account for the variations in partial melting as determined from trace element analyses. In particular, two fundamental observations cannot be reconciled with the model based on isotopic ratios

alone. First, according to Werner *et al.* (2003), the Costa Rica Seamounts are considered genetically similar to lavas from the northern Galápagos archipelago [the 'Northern Domain' of Hoernle *et al.* (2000)], but their alkalic, highly ITE-enriched compositions bear little resemblance to lavas erupted along the Wolf–Darwin Lineament (Fig. 1).

The second unexplained observation is the formation of the lavas erupted on and around Cocos Island. According to Werner *et al.* (2003), the Cocos Island Province is associated with compositions observed in the middle of the Galápagos archipelago today [the 'Central Domain' of Hoernle *et al.* (2000)], because of their isotopic resemblance to lavas erupted at Fernandina Island. Yet both Cocos Island and the surrounding seamount lavas have ITE concentrations far more enriched than any observed on the Galápagos Platform and exhibit almost exclusively alkalic compositions. Moreover, Bellon *et al.* (1984) established that Cocos Island was produced within the past ~2 Myr, hence it must have been erupted over 500 km from the presumed plume center in the western Galápagos archipelago. Castillo *et al.* (1988) concurred that Cocos Island was constructed far from the Galápagos plume center, possibly as the result of reactivation of small-degree Galápagos plume melts. Meschede & Barckhausen (2000) took these observations a step further and attributed the Cocos Island lavas to a second hotspot isolated beneath the Cocos Plate.

Failed rifts and alkalic seamount provinces

Both the Costa Rica and Cocos Island Provinces are located on or near extinct spreading centers (Meschede & Barckhausen, 2000). The northeastern end of the Cocos Ridge is the site of an extinct spreading center abandoned when the GSC began a southward jump at ~19·5 Ma (Meschede & Barckhausen, 2000). Consequently, the Costa Rica Seamounts are clustered around the NW end of the abandoned rift.

Werner *et al.* (1999) dated lavas dredged along the eastern half of the Costa Rica Seamount Province, parallel to the Costa Rican coast, revealing ages ranging from 12·97 ± 0·21 Ma to 14·46 ± 0·32 (1σ) Ma. According to paleomagnetic data, the lithosphere underlying this seamount province is older than 15 Ma (Meschede & Barckhausen, 2000). The seamounts, therefore, were not produced at the active ridge axis, but later, after the GSC had jumped south. All the Costa Rica seamounts are clustered within ~200 km of the abandoned spreading center (Fig. 1).

Likewise, the Cocos Island Province is also located adjacent to a failed spreading center. Unfortunately, the ages of the seamounts around Cocos Island are not known, but K–Ar ages of Dalrymple & Cox (1968) and Bellon *et al.* (1984) indicate that the subaerial parts of the island are <2 Ma, at least 5 Myr younger than the underlying lithosphere [based on plate motion vectors of Wilson (1996) and Barckhausen *et al.* (2001)]. It is not unreasonable to posit that the seamounts clustered around Cocos Island were formed during broadly the same timeframe, because the compositions of the seamount lavas closely resemble those of Cocos Island, in their extreme ITE enrichment, alkalic compositions, and nearly identical isotopic and ITE ratios (Castillo *et al.*, 1988; Werner *et al.*, 2003).

According to Meschede & Barckhausen (2000), the Cocos Island region is the site of a failed rift. An east–west-trending spreading center became active at ~3·5 Ma, but went extinct by ~2 Ma, leaving an abandoned rift extending westward *c.* 200 km from the region near Cocos Island. Thus, if the Cocos Island Province formed nearly contemporaneously with Cocos Island, then the seamounts were erupted shortly after the failure of the rift, and they all formed within 200 km of the abandoned segment.

Abundant post-abandonment alkalic volcanism, lasting for several million years after a ridge jump, appears to be a common feature of failed rifts. Batiza & Vanko (1985) proposed that as rifting activity slows, magma supply to the ridge becomes sporadic and a steady-state magma chamber can no longer exist, resulting in abundant strongly evolved lavas, just as is observed in the Cocos Province. After the cessation of spreading, alkali basalts are produced by low degrees of melting, which are a manifestation of the progressively thickening lithosphere as the region cools.

The Mathematician Ridge is a ~800 km long failed rift located north of the Cocos Ridge in the eastern Pacific (e.g. Mammerickx *et al.*, 1988). At *c.* 3·5 Ma, activity along the ridge shifted eastward nearly 600 km to what is now the East Pacific Rise at 10°–20°N (e.g. Mammerickx & Klitgord, 1982). The region around the Mathematician Ridge is notable for abundant alkalic seamounts and islands (Socorro, San Benedicto, Clarion, and Roca Partida) that form the Revillagigedo Archipelago (e.g. Bohrson & Reid, 1995). Fieldwork and dredging operations have revealed that the subaerial and submarine volcanoes throughout the area remain active today (Farmer *et al.*, 1993; McClelland *et al.*, 1993; Bohrson & Reid, 1995; Bohrson *et al.*, 1996), producing alkalic lavas that appear to be derived from similar mantle sources (Batiza & Vanko, 1985; Bohrson & Reid, 1995, 1997). The active volcanic region is broad, extending across the entire failed rift and transform system and up to 350 km SW of Clarion Island (Batiza & Vanko, 1985).

The lavas of both the Costa Rica and Cocos Island Provinces bear a striking resemblance to those erupted from the Mathematician Ridge and the related islands (Batiza & Vanko, 1985; Bohrson & Reid, 1995, 1997, 1998; Bohrson *et al.*, 1996): (1) with the exception of a few tholeiitic lavas in the Costa Rica Province, all lavas

erupted in the failed rift regions are alkalic; (2) subaerial lavas exhibit greater degrees of differentiation than the seamounts, extending to trachytic compositions on Cocos Island (e.g. Castillo *et al.*, 1988; Socorro Island lavas include abundant peralkaline trachytes and rhyolites; Bohrson & Reid, 1995, 1997); (3) magmatism persisted at the same place long enough for the volcanic structures to emerge as islands; (4) both the subaerial and the seamount lavas in a given province are derived from either the same or similar mantle sources, with limited ranges in radiogenic isotope and ITE ratios (Bohrson & Reid, 1995, 1997); (5) high field strength element (HFSE) concentrations increase systematically with decreasing MgO content, whereas ratios of HFSE remain relatively constant for the submarine samples (Cocos Island lavas exhibit significant variation in HFSE ratios with MgO; Fig. 7).

Some of the trace element compositions of Cocos and Costa Rica seamount lavas share features that Bohrson & Reid (1995, 1997) attributed to assimilation of oceanic crust: (1) incompatible elements including Ba and Y do not correlate well with incompatible HFSE, instead exhibiting two distinct trends (Fig. 7b), an indication of assimilation taking place in addition to straightforward fractional crystallization (Bohrson & Reid, 1995); (2) like Socorro Island lavas, the Cocos and Costa Rica Seamount Province lavas exhibit highly variable Ba, P_2O_5, and Y contents for a given MgO content, as well as a spectrum of negative Ce anomalies, a phenomenon Bohrson & Reid (1995) attributed to variable assimilation of ocean crust.

Given the extensive petrologic and geochemical similarities to lavas erupted in the Mathematician Ridge region, we propose that the Costa Rica and Cocos Island Provinces are also the manifestation of failed rifts. This conclusion is further strengthened by the proximity of the seamount provinces to abandoned spreading center scars (Meschede & Barckhausen, 2000), as well as the timing of their eruption relative to that of the major spreading center jumps (beginning at 19·5 Ma: Costa Rica Province; ~2–3 Ma: Cocos Island Province; Bellon *et al.*, 1984; Werner *et al.*, 1999; Meschede & Barckhausen, 2000).

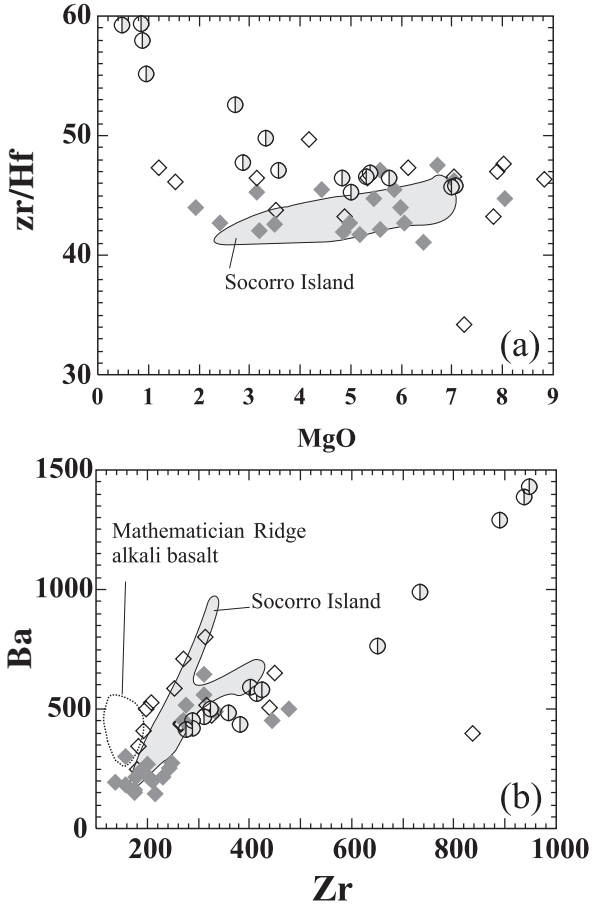

Fig. 7. Comparison of aseismic ridge data with Socorro Island (post-caldera mafic volcanics only, including alkali basalts, hawaiites and mugearites, but not the trachytes or rhyolites) and Mathematician Ridge lavas [fields from Bohrson & Reid (1995)]. (a) Zr/Hf vs MgO (Werner *et al.*, 2003); (b) Ba vs Zr. Symbols as in Fig. 2.

Melt generation and failed rift systems

We propose that the predominantly alkalic Cocos and Costa Rica Seamount Provinces are the result of post-abandonment volcanism, following jumps and the failure of a spreading ridge in each of the regions. The mechanism for widely dispersed alkalic volcanism after a spreading ridge jump has occurred can be explained as the result of the decrease in the upwelling rate. As spreading ridge activity wanes, decreased upwelling will result in progressively lower extents of melting. Furthermore, far-field, deviatoric stresses generated by major tectonic rearrangements may also cause extensive cracking of the lithosphere in the vicinity of the failing rift, as has been observed in Iceland (e.g. Fujita & Sleep, 1978; Clifton *et al.*, 2000). The stress field could result in the initiation of mantle upwelling, causing widespread, localized volcanic activity over a period lasting up to several million years from initial spreading rift failure (Batiza & Vanko, 1985).

In this model, each volcanic center taps only the immediately underlying mantle, consistent with geochemical observations that the seamounts are derived from variable amounts of partial melting of similar mantle sources. The elongate structures and linear arrangements of many of the seamounts in the Costa Rica and Cocos Provinces further support the idea that they may result from volcanism caused by rifting and upwelling; such asymmetric structural features are relatively rare in off-axis seamount provinces (Batiza & Vanko, 1983; Smith & Cann, 1992) and are indicative of unusually strong deviatoric stresses

on a regional scale. It should also be noted that both the Costa Rica and Cocos Island Provinces are located on the northern flanks of the main Cocos Ridge, not on the crest itself, where the bulk of the hotspot-produced lavas have presumably accumulated. The off-axis location of the seamounts is therefore more consistent with the failed rift origin than as direct products of the Galápagos plume. Nevertheless, as described by Werner *et al.* (2003), we believe that the Galápagos plume is responsible for the majority of the aseismic ridges' volume.

Broadly similar, tensional volcanism has also been invoked to explain the distribution and composition of islands and seamounts in the northern Galápagos archipelago (Harpp & Geist, 2002; Harpp *et al.*, 2002). An important difference between the northern Galápagos and the aseismic ridge seamount provinces, however, is that only tholeiitic lavas have been produced in the northern Galápagos and none of the volcanoes' compositions achieve the ITE enrichment of the Cocos Ridge seamounts (Harpp & Geist, 2002). We attribute this distinction to the fundamental difference between the two tectonic settings. In the northern Galápagos, the active region is bounded by the Galápagos plume to the south and an active spreading center to the north. Consequently, the ambient temperature of the mantle throughout the northern Galápagos should be higher than average, resulting in abundant melt supply to the volcanic centers. Lavas in the northern Galápagos exhibit $(Sm/Yb)_n > 1$, an indication that the melts were partially generated in the garnet stability field.

Isotopically, however, the depleted mantle plays a significant role in all the northern Galápagos compositions (Harpp & White, 2001). The elevated sub-lithospheric temperatures throughout this region, therefore, not only cause partial melting of fertile mantle heterogeneities, such as pockets of PLUME source dispersed in the mantle (Harpp & Geist, 2002), but they also initiate melting of the depleted upper mantle, which dilutes the magmas to the observed intermediate enrichment levels. In the seamount provinces on the Cocos Ridge, ambient mantle temperatures are lower, minimizing the contribution from the more refractory depleted mantle source and allowing the small-degree, alkalic melts of enriched material to dominate erupted compositions.

Extensive studies of the present-day GSC have established that lavas erupted along the mid-ocean ridge axis within a few hundred kilometers of the hotspot are contaminated by the Galápagos plume (e.g. Schilling *et al.*, 1982, 2003; Detrick *et al.*, 2002). Lithosphere and sub-lithospheric mantle produced at the GSC in the past, when the plume–GSC separation was equal to or less than it is today, should similarly be infused with plume material. Therefore, the volcanic centers of the Cocos and Costa Rica Seamount Provinces tap mantle that is variably contaminated with plume material. Because the enriched plume source is more fertile than the surrounding depleted mantle, it should be the first to melt, and in a region of only limited heat supply such as a failed rift, may be the only material that is ultimately erupted.

Revised tectonic model

We propose the following sequence of tectonic and volcanic events that summarize the ~20 Myr history of interaction between the Galápagos plume and Galápagos Spreading Center (Fig. 8), amended from Werner *et al.* (2003).

(1) *~19·5–14·5 Ma.* At *c.* 19·5 Ma, the Galápagos Spreading Center began a ~20° strike shift in a major tectonic rearrangement (Meschede *et al.*, 1998; Barckhausen *et al.*, 2001). The alkalic volcanoes of the Costa Rica Seamount Province then erupted over an interval of several million years as the abandoned spreading center failed (e.g. Batiza & Vanko, 1985). The waning upwelling rate resulted in small amounts of deep melting of a predominantly PLUME source, yielding alkalic lavas highly enriched in incompatible trace elements. During this period, the bulk of the hotspot products were being deposited onto the Nazca Plate, forming the combined Carnegie and Malpelo Ridges from moderate degrees of partial melting in the garnet stability field of a predominantly PLUME–DUM mantle source, much like lavas erupted today in the central Galápagos archipelago.

(2) *14·5–12 Ma.* The GSC again jumped south, with a minor change in strike (Meschede *et al.*, 1998; Barckhausen *et al.*, 2001), causing the ridge to overlap only the southern edge of the hotspot. Consequently, the volume of eruptive material deposited on the Nazca Plate decreased, manifested as a narrowing of the Carnegie Ridge between 85°W and 87°W (Fig. 8). The southward GSC jump also caused the Malpelo Ridge to initiate rifting away from the Carnegie Ridge. Beginning at this time, the bulk of the hotspot products were erupted onto the Cocos Plate, the results of slightly higher extents of melting in the garnet stability field (2–10%), with a greater contribution from PLUME than in the past, much like lavas erupted at the western Galápagos shield volcanoes today. Because the plume was located predominantly beneath the Cocos Plate during this interval, the Cocos Ridge axis reflects the geochemical zonation of the Galápagos plume (Hoernle *et al.*, 2000; Werner *et al.*, 2003).

(3) *12–11 Ma.* Werner *et al.* (2003) proposed that the Galápagos plume was centered beneath an offset in the GSC at this time, because only lavas with PLUME-like compositions are observed along the Cocos Ridge. This minor change in the GSC configuration is reflected in a shift in the strike of the magnetic sea-floor anomalies for this period (Barckhausen *et al.*, 2001) and probably marks the initiation of northward migration of the GSC that continues today (Wilson & Hey, 1995).

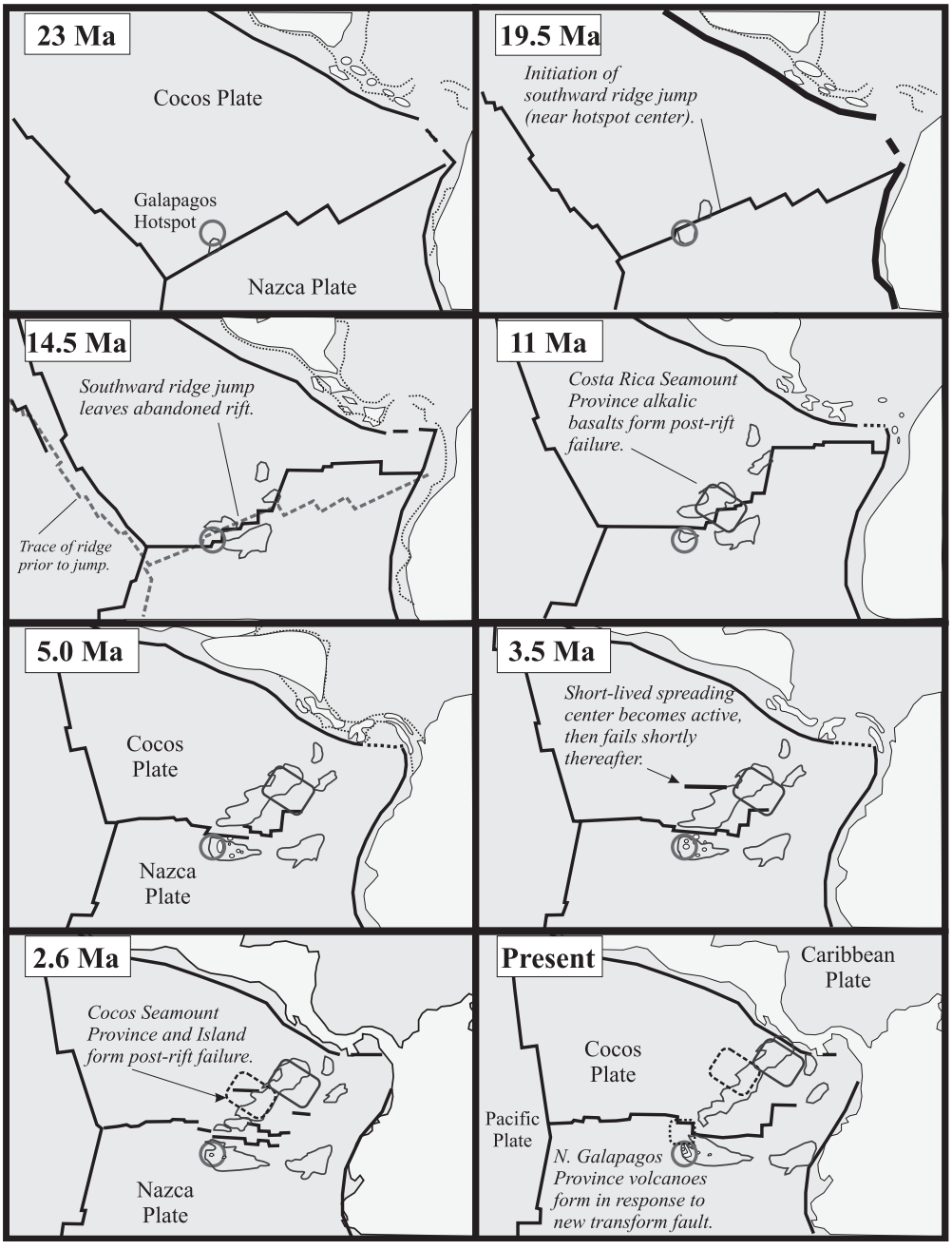

Fig. 8. Tectonic reconstruction modified from Meschede & Barckhausen (2000); 5·2 and 2·6 Ma from Wilson & Hey (1995). Fine dotted lines are backtracked topography for reference (Meschede & Barckhausen, 2000). Bold dashed line in 14·5 Ma scenario is a trace of the previous ridge location prior to the reorientation at 14·5 Ma, also for reference. Box (continuous line) that appears at 11 Ma represents initiation and subsequent formation of Costa Rica Seamount Province in response to the ridge jump initiated at 19·5 Ma. Box (dashed line) that appears at 2·6 Ma represents formation of the Cocos Seamount Province and Cocos Island, after rift formation and failure at ~3·5 Ma. Box (dotted line) in 'Present' delineates the Northern Galápagos Province (including the Wolf–Darwin Lineament), which may have begun formation after the 91°W transform fault was initiated at ~3·5 Ma (Wilson & Hey, 1995).

(4) *~9·5 Ma.* Spreading between the Malpelo and Carnegie Ridges ceased around this time.

(5) *5·2–~3·5 Ma.* The GSC moved north of the plume center during this period (Wilson & Hey, 1995), shifting the eruption of hotspot material onto the Nazca Plate in its entirety, similar to the current hotspot–ridge configuration.

(6) *~3·5–2 Ma.* A short-lived, east–west-trending spreading center became active north of the GSC (Meschede & Barckhausen, 2000). Shortly thereafter,

this rift failed, resulting in the post-abandonment alkalic volcanism responsible for the ~2 Ma formation of Cocos Island (Castillo *et al.*, 1988) and the surrounding Cocos Island Province seamounts. Once again, only deep, small-degree melts of a predominantly PLUME mantle source were generated as the rift's magma supply was cut off.

(7) *~2·6 Ma.* A major transform fault formed immediately north of the hotspot, probably the result of a southward jump by the GSC segment closest to the plume (e.g. Small, 1995; Wilson & Hey, 1995). The regional stresses initiated widespread, dispersed volcanism throughout the northern Galápagos, resulting in the formation of the tholeiitic islands and seamounts of the Wolf–Darwin Lineament and northern Galápagos (Harpp & Geist, 2002; Harpp *et al.*, 2002). The elevated mantle temperatures caused by the adjacent ridge and plume systems initiated melting of the depleted mantle and lowered average depths of melting.

(8) *Present.* The geochemical zonation of the Galápagos plume is detectable along the western periphery of the platform (White *et al.*, 1993; Kurz & Geist, 1999; Harpp & White, 2001). According to Hoernle *et al.* (2000), the central part of the archipelago is covered by lavas with a more depleted signature as the Nazca Plate moves eastward, leaving the altered, southern plume component detectable on the southern flank of the Carnegie Ridge (Werner *et al.*, 2003).

CONCLUSIONS

Trace element analyses of dredged samples collected along the Cocos, Carnegie, Coiba, and Malpelo Ridges during the PAGANINI expedition provide important insights into the history of the Galápagos hotspot and plume–ridge interaction over the past ~20 Myr. The compositional and spatial trends in the aseismic ridge data suggest that the Galápagos plume has been compositionally zoned for the past ~18–20 Myr (Werner *et al.*, 2003), exhibiting the same spatial zonation as the present-day Galápagos archipelago (e.g. Geist *et al.*, 1988; White *et al.*, 1993; Harpp & White, 2001). The dynamic relationship between the plume and the ridge, however, adds an additional set of complexities to the system, resulting in deviations from the predicted distribution of compositions along the Cocos and Carnegie Ridges caused by a zoned plume (Hoernle *et al.*, 2000).

On the basis of regional variations in melting conditions along the ridges, as determined from the trace element contents of the dredged lavas, the relationship between the Galápagos plume and the Galápagos Spreading Center can be elucidated. Trace element content variations are generally consistent with the tectonic history of the plume–GSC system as proposed by Werner *et al.* (2003; Fig. 8), with some modifications to take into account volcanism following the failure of spreading ridge systems.

The Costa Rica Province seamounts probably formed within a few million years after the major ridge jump at 19·5 Ma (e.g. Meschede & Barckhausen, 2000). They are the result of waning mantle upwelling in response to regional deviatoric stresses after the jump. Similarly, Cocos Island and the surrounding seamounts may have formed in the wake of a ridge failure at ~2 Ma (e.g. Bellon *et al.*, 1984) instead of a second hotspot center (e.g. Meschede & Barckhausen, 2000). Tests of this hypothesis would include geochronological analysis of the lavas from the Costa Rica and Cocos Island Provinces, which should each cluster within a few million years of the ridge jumps at 19·5 and 2 Ma.

Aseismic ridges and their associated seamounts, therefore, are not simply the surficial manifestation of plume activity, but also reflect subsequent regional tectonic events, including spreading center jumps and migration. They may serve as valuable sources of information about the history of a mantle plume. In the presence of a proximal spreading center, aseismic ridges preserve a record of the interaction between the spreading center and the hotspot that permits reconstruction of the regional tectonic history.

ACKNOWLEDGEMENTS

We would like to thank the scientific team and shipboard crew of the R.V. *Sonne* during the SO 144-3 PAGANINI expedition for their assistance in carrying out this study. We also thank L. Mayhew for sample preparation efforts. In addition, Britta Lissinna provided the Colgate students with invaluable assistance and hospitality while they were processing samples for analysis at GEOMAR. We extend our gratitude to the governments of Costa Rica and Ecuador for granting access to their territorial waters and to Cocos Island. Thanks go to Wendy Bohrson, Dennis Geist, and Pat Castillo for their thoughtful and constructive reviews. This study was supported by NSF grants CHE-9996141 and CHE-9996136 to K.S.H.; cruise funding was provided by the German Ministry of Education and Research (BMBF; Grant PAGANINI).

SUPPLEMENTARY DATA

Supplementary data for this paper are available at *Journal of Petrology* online.

REFERENCES

Barckhausen, U., Ranero, C. R., von Huene, R., Cande, S. C. & Roeser, H. A. (2001). Revised tectonic boundaries in the Cocos plate off Costa Rica: implications for the segmentation of the convergent

margin and for plate tectonic models. *Journal of Geophysical Research* **106**, 19207–19220.

Batiza, R. & Vanko, D. A. (1985). Petrologic evolution of large failed rifts in the eastern Pacific: petrology of volcanic and plutonic rocks from the Mathematician ridge area and the Guadalupe trough. *Journal of Petrology* **26**, 564–602.

Bellon, H., Saenz, R. & Tournon, J. (1984). K–Ar radiometric ages of lavas from Cocos Island (eastern Pacific). *Marine Geology* **54**, M17–M23.

Blichert-Toft, J. & White, W. M. (2001). Hf isotope geochemistry of the Galápagos Islands. *Geochemistry, Geophysics, Geosystems* **2**, paper number 2000GC00138, posted at http://www.g-cubed.org.

Bohrson, W. A. & Reid, M. R. (1995). Petrogenesis of alkaline basalts from Socorro Island, Mexico: trace element evidence for contamination of ocean island basalt in the shallow ocean crust. *Journal of Geophysical Research* **100**, 24555–24576.

Bohrson, W. A. & Reid, M. R. (1997). Genesis of silicic peralkaline volcanic rocks in an ocean island setting by crustal melting and open-system processes: Socorro Island, Mexico. *Journal of Petrology* **38**, 1137–1166.

Bohrson, W. A. & Reid, M. R. (1998). Genesis of evolved ocean island magmas by deep- and shallow-level basement recycling, Socorro Island, Mexico: constraints from Th and other isotope signatures. *Journal of Petrology* **39**, 995–1008.

Bohrson, W. A., Reid, M. R., Grunder, A. L., Heizler, M. T., Harrison, T. M. & Lee, J. (1996). Prolonged history of silicic peralkaline volcanism in the eastern Pacific Ocean. *Journal of Geophysical Research* **101**, 11457–11474.

Castillo, P., Batiza, R., Vanko, D., Malavassi, E., Barquero, J. & Fernandez, E. (1988). Anomalously young volcanoes on old hot-spot traces: I. Geology and petrology of Cocos Island. *Geological Society of America Bulletin* **100**, 1400–1414.

Christie, D. M., Duncan, R. A., McBirney, A. R., Richards, M. A., White, W. M., Harpp, K. S. & Fox, C. G. (1992). Drowned islands downstream from the Galápagos hotspot imply extended speciation times. *Nature* **355**, 246–248.

Clifton, A. E., Schlische, R. W., Withjack, M. O. & Ackermann, R. V. (2000). Influence of rift obliquity on fault-population systematics: results of experimental clay models. *Journal of Structural Geology* **22**, 1491–1509.

Dalrymple, G. B. & Cox, A. (1968). Paleomagnetism, potassium–argon ages and petrology of some volcanic rocks. *Nature* **217**, 323–326.

Detrick, R. S., Sinton, J. M., Ito, G., Canales, J. P., Behn, M., Blacic, T., Cushman, B., Dixon, J. E., Graham, D. W. & Mahoney, J. J. (2002). Correlated geophysical, geochemical, and volcanological manifestations of plume–ridge interaction along the Galápagos Spreading Center. *Geochemistry, Geophysics, Geosystems* **3**, 8501, doi: 10.1029/2002GC000350, posted at http://www.g-cubed.org.

Doherty, W. (1989). Internal standardization procedure for the determination of yttrium and the rare earth elements in geological materials by inductively coupled plasma-mass spectrometry. *Geochimica et Cosmochimica Acta* **44B**, 263–280.

Eggins, S. M., Woodhead, J. D., Kinsley, L. P. J., Mortimer, G. E., Sylvester, P., McCulloch, M. T., Hergt, J. M. & Handler, M. R. (1997). A simple method for the precise determination of 40 trace elements in geological samples by ICP-MS using enriched isotope internal standardization. *Chemical Geology* **134**, 311–326.

Farmer, J. D., Farmer, M. C. & Berger, R. (1993). Radiocarbon ages of lacustrine deposits in volcanic sequences of the Lomas Coloradas area, Socorro Island, Mexico, *Radiocarbon* **35**, 253–262.

Fujita, K. & Sleep, N. (1978). Membrane stresses near mid-ocean ridge–transform intersections. *Tectonophysics* **50**, 207–221.

Gallahan, W. E. & Nielsen, R. L. (1992). The partitioning of Sc, Y, and the rare earth elements between high-Ca pyroxene and natural mafic to intermediate lavas at 1 atmosphere. *Geochimica et Cosmochimica Acta* **56**, 2387–2404.

Geist, D. J., White, W. M. & McBirney, A. R. (1988). Plume asthenosphere mixing beneath the Galápagos Archipelago. *Nature* **333**, 657–660.

Geldmacher, J., Hanan, B. B., Blichert-Toft, J., Harpp, K., Hoernle, K., Hauff, F., Werner, R. & Kerr, A. C. (2003). Hafnium isotopic variations in volcanic rocks from the Caribbean Large Igneous Province and Galápagos hot spot tracks. *Geochemistry, Geophysics, Geosystems* **4**(7), 1062, doi: 10.1029/200296000477.

GERM Website, http://earthref.org/GERM/, last updated 29 May 2003; accessed 6 July 2003.

Gripp, A. E. & Gordon, R. G. (1990). Current plate velocities relative to hotspots incorporating the NUVEL-1 global plate model. *Geophysical Research Letters* **11**, 1109–1112.

Harpp, K. S. (1995). Magmatic evolution of mid-ocean ridges and hotspots: isotopic and trace element studies of the East Pacific Rise, Mid-Atlantic Ridge, and Galápagos Islands. Ph.D. thesis, Cornell University, Ithaca, NY.

Harpp, K. S. & Geist, D. J. (2002). Wolf–Darwin lineament and plume–ridge interaction in northern Galápagos. *Geochemistry, Geophysics, Geosystems* **3**, 8504, doi: 10.1029/2002GC000370, posted at http://www.g-cubed.org.

Harpp, K. S. & White, W. M. (2001). Tracing a mantle plume: isotopic and trace element variations of Galápagos seamounts. *Geochemistry, Geophysics, Geosystems* **2**, paper number 2000GC00137, posted at http://www.g-cubed.org.

Harpp, K. S., Wirth, K. R. & Korich, D. J. (2002). Northern Galápagos Province: hotspot-induced, near-ridge volcanism at Genovesa Island. *Geology* **30**, 399–402.

Hey, R. (1977). Tectonic evolution of the Cocos–Nazca spreading center. *Geological Society of America Bulletin* **88**, 1404–1420.

Hoernle, K., Werner, R., Phipps Morgan, J., Garbe-Schonberg, D., Bryce, J. & Mrazek, J. (2000). Existence of complex spatial zonation in the Galápagos plume for at least 14 m.y. *Geology* **28**, 435–438.

Hoernle, K., van den Bogaard, P., Werner, R., Hauff, F., Lissinna, B., Alvarado, G. E. & Garbe-Schönberg, D. (2002). Missing history (16–71 Ma) of the Galápagos hotspot: implications for the tectonic and biological evolution of the Americas. *Geology* **30**, 795–798.

Holden, J. C. & Dietz, R. S. (1972). Galápagos Gore, NazCoPac Triple Junction and Carnegie/Cocos Ridges. *Nature* **100**, 266–269.

Kellogg, J. N. & Vega, V. (1995). Tectonic development of Panama, Costa Rica, and the Colombian Andes: constraints from global positioning system geodetic studies and gravity. In: Mann, P. (ed.) *Geologic and Tectonic Development of the Caribbean Plate Boundary in Southern Central America*. Boulder, CO: Geological Society of America, pp. 75–90.

Kurz, M. D. & Geist, D. (1999). Dynamics of the Galápagos hotspot from helium isotope geochemistry. *Geochimica et Cosmochimica Acta* **63**, 4139–4156.

Langmuir, C. H., Voche, R. D., Jr, Hanson, G. N. & Hart, S. R. (1978). A general mixing equation with applications to Icelandic basalts. *Earth and Planetary Science Letters* **37**, 380–392.

Langmuir, C. H., Klein, E. M. & Plank, T. (1992). Petrological systematics of mid-ocean ridge basalts: constraints on melt generation beneath ocean ridges. In: Morgan, J. P., Blackman, D. K. & Sinton, J. M. (eds) *Mantle Flow and Melt Generation at Mid-Ocean Ridges*. *Geophysical Monograph, American Geophysical Union*, **71**, 183–280.

Lonsdale, P. & Klitgord, K. D. (1978). Structure and tectonic history of the eastern Panamá Basin. *Geological Society of America Bulletin* **89**, 981–999.

Mammerickx, J. & Klitgord, K. D. (1982). Northern East Pacific Rise; magnetic anomaly and bathymetric framework. *Journal of Geophysical Research B*, **87**, 6725–6750.

Mammerickx, J., Naar, D. F. & Tyce, R. L. (1988). The Mathematician paleoplate. *Journal of Geophysical Research* **93**, 3025–3040.

Meschede, M. & Barckhausen, U. (2000). Plate tectonic evolution of the Cocos–Nazca spreading center. In: Silver, E. A., Kimura, G. & Shipley, T. H. (eds) *Proceedings of the Ocean Drilling Program, Scientific Results, 170*. College Station, TX: Ocean Drilling Program [online]. Posted at http://www-odp.tamu.edu/publications/170_SR/chap_07/chap_07.htm. Accessed 7 July 2003.

Meschede, M., Barckhausen, U. & Worm, H.-U. (1998). Extinct spreading on the Cocos Ridge. *Terra Nova* **10**, 211–216.

Morgan, W. J. (1971). Convection plumes in the lower mantle. *Nature* **230**, 42–43.

Schilling, J.-G., Kingsley, R. H. & Devine, J. D. (1982). Galápagos hot spot–spreading center system: 1. Spatial petrological and geochemical variations (83°W–101°W). *Journal of Geophysical Research* **87**, 5593–5610.

Schilling, J.-G., Fontignie, D., Blichert-Toft, J., Kingsley, R. & Tomza, U. (2003). Pb–Hf–Nd–Sr isotope variations along the Galápagos Spreading Center (101°–83°W): constraints on the dispersal of the Galápagos mantle plume. *Geochemistry, Geophysics, Geosystems* **4**, 512, doi: 10.1029/2002GC000495, posted at http://www.g-cubed.org.

Sinton, C., Christie, D. M. & Duncan, R. A. (1996). Geochronology of Galápagos seamounts. *Journal of Geophysical Research* **101**, 13689–13700.

Small, C. (1995). Observations of ridge–hotspot interactions in the Southern Ocean. *Journal of Geophysical Research B* **100**, 17931–17946.

Smith, D. K. & Cann, J. R. (1992). The role of seamount volcanism in crustal construction at the Mid-Atlantic Ridge (24°–30°N). *Journal of Geophysical Research B* **97**, 1645–1658.

Smith, W. H. F. & Sandwell, D. T. (1997). Global seafloor topography from satellite altimetry and ship depth soundings. *Science* **277**, 1956–1962.

Sun, S. S. & McDonough, W. F. (1989). Chemical and isotopic systematics of oceanic basalts; implications for mantle composition and processes. In: Saunders, A. D. & Norry, M. J. (eds) *Magmatism in the Ocean Basins. Geological Society, London, Special Publications* **42**, 313–345.

Van Andel, T.H., Heath, G. R. Malfait, B. T., Heinrichs, D. F. & Ewing, J. I. (1971). Tectonics of the Panama Basin, eastern equatorial Pacific. *Geological Society of America Bulletin* **82**, 1482–1504.

Walther, C. H. E. (2003). The structure of the Cocos Ridge off Costa Rica. *Journal of Geophysical Research* **108**, doi: 10.1029/2001LB000888.

Werner, R., Hoernle, K., v.d. Bogaard, P., Ranero, C., von Huene, R. & Korich, D. (1999). Drowned 14 m.y.-old Galápagos Archipelago off the coast of Costa Rica: implications for tectonic and evolutionary models. *Geology* **27**, 499–502.

Werner, R., Hoernle, K., Barckhausen, U. & Hauff, F. (2003). Geodynamic evolution of the Galápagos hot spot system (Central East Pacific) over the past 20 m.y.: constraints from morphology, geochemistry, and magnetic anomalies. *Geochemistry, Geophysics, Geosystems* **4**, 1108, doi: 10.1029/2003GC000576, posted at http://www.g-cubed.org.

White, W. M. & Hofmann, A. W. (1978). Geochemistry of the Galápagos Islands: implications for mantle dynamics and evolution. *Carnegie Institute of Washington Yearbook* **77**, 596–606.

White, W. M., McBirney, A. R. & Duncan, R. A. (1993). Petrology and geochemistry of the Galápagos Islands: portrait of a pathological mantle plume. *Journal of Geophysical Research* **98**, 19533–19563.

Wilson, D. S. (1996). Fastest known spreading on the Miocene Cocos–Pacific plate boundary. *Geophysical Research Letters* **23**, 3003–3006.

Wilson, D. S. & Hey, R. N. (1995). History of rift propagation and magnetization intensity for the Cocos–Nazca spreading center. *Journal of Geophysical Research* **100**, 10041–10056.

Wood, D. A. (1980). The application of a Th–Hf–Ta diagram to problems of tectonomagmatic classification and to establishing the nature of crustal contamination of basaltic lavas of the British Tertiary volcanic province. *Earth and Planetary Science Letters* **50**, 11–30.